

How asymmetries in the feedforward signals
are exploited by target neurons to elaborate
feature selectivity

Yamni Mohan

Abstract

This is the abstract of my thesis

Contents

1 Acknowledgements	5
2 Abstract	6
3 Introduction	7
4 Methods	9
4.1 Experimental Animals	9
4.2 Surgery and Anaesthesia	10
4.3 Electrophysiological Recordings	12
4.3.1 Single Electrode Recordings	12
4.3.2 Multielectrode Recordings	13
4.4 Stimuli	14
4.5 Data Analysis	15
4.6 Histology	19
4.6.1 Cresyl violet staining	20
4.6.2 Track Reconstruction	20

4.7	Optical Imaging of Intrinsic Signals	21
4.7.1	The apparatus	21
4.7.2	Image acquisition	23
4.7.3	Analysis of Intrinsic Signals	24
5	Radial Bias in large spatial scale optical imaging signal in the macaque Primary Visual Cortex	28
5.1	Summary	29
5.2	Introduction	30
5.3	Methods	33
5.4	Results	43
5.5	Discussion	54
5.6	Conclusion	60
6	Orientation tuning in the Tree Shrew superior colliculus	61
6.1	Abstract	62
6.2	Introduction	63
6.3	Methods	65
6.3.1	Electrophysiology	65
6.3.2	Stimuli	66
6.3.3	Data Analysis	68
6.4	Results	69
6.5	Discussion	74
6.5.1	Anatomical Relevance	76

6.5.2	Comparison with previous tree shrew studies	78
6.5.3	Comparison with previous superior colliculus studies .	80
6.5.4	Comparison with the geniculostriate system of cats and macaques	81
6.5.5	Conclusion	82
7	Is the tree shrew primary visual cortex a linear filter?	83
7.1	Summary	84
7.2	Introduction	85
7.3	Methods	89
7.3.1	Surgery and Anaesthesia	89
7.3.2	Electrophysiology	90
7.3.3	Stimuli	91
7.3.4	Data Analysis	92
7.3.5	Histology	94
7.4	Results	95
7.5	Discussion	101
References		106

Chapter 1

Acknowledgements

Chapter 2

Abstract

Chapter 3

Introduction

Over the years, sub-cortical orientation biases have been shown to play a significant role in two key areas of study in the primary visual cortex. The first is its role in generating sharp orientation selectivity in the cortex and second is its role in generating the cortical architecture. In my thesis, I aim to further characterise the sub-cortical orientation biases and examine their role in visual processing. In the first part of my thesis, I would like to characterise the origin of the biased sub-cortical input to the cortex. There is debate as to exactly when in visual processing the orientation bias observed in the cortical input is generated. Some studies claim that this orientation bias is generated early on in the visual processing: namely the retina. Some others claim that these biases are generated through a mechanism such as excitatory convergence in the cortex. This part probes this question in two ways.

Chapter 6

This chapter examines if there is a preponderance of a particular orientation in the cortical inputs. If the orientation bias in the cortical input is generated by Hubel and Wiesel type excitatory convergence — where circular LGN receptive fields converge on to a V1 neuron — we would expect that inputs to the cortex don't show any preferences (i.e. the orientations of the inputs will be randomly distributed.). Many studies however, have shown that RGCs and LGN neurons are preferentially tuned to the radial orientation (the orientation of the line joining the center of the receptive field to the centre of visual field). If the orientation bias in the inputs is derived from the retina instead, then this

Chapter 4

Methods

4.1 Experimental Animals

All experimental procedures were approved by the Florey Institute Animal Ethics committee and were conducted in accordance with the guidelines from the Animal Welfare Act 1992, The Animal Welfare Regulations (Vic) 1993 and the National Health & Medical Research Councils (NHMRC) Australian Code of Practice for the Care and Use of Animals for Scientific Purposes (8th Edition, listed as EA28 in the NHMRC Publications Online Catalogue under Animal Ethics). This study looked at the responses to visual stimuli in macaques (*Macaca nemestrina*) and tree shrews (*Tupaia glis*). The macaques were transported from the macaque colony (Monash Animal Research Platform) to the Melbourne Brain Centre (MBC) the day before the experiment and housed overnight and experimented on from the following day onwards.

The tree shrews were obtained from the tree shrew colony at the MBC funded by the ARC Centre of Excellence in Integrative Brain Function. Macaque experiments typically lasted for 5 days and Tree Shrew experiments for 2 days. Data for this thesis was collected from a total of 6 macaques and 16 tree shrews.

4.2 Surgery and Anaesthesia

In all animals, initial anaesthesia was induced using a mixture of Ketamine (KETAMIL, Parnell Lab, Australia) and Xylazine (ILIUM XYLAZIL-20, Troy Laboratories, Australia; See table 1 for dosage). Once the animals were anaesthetised, venous cannulation was performed to help administer drugs and fluids. Following this, a tracheostomy was performed to administer artificial ventilation and anaesthesia during the experiment. Once the venous cannulation and tracheostomy were completed, the animals were mounted on a stereotaxic table in Horsley-Clarke co-ordinates. Artificial ventilation was provided using a respiratory pump (Harvard Apparatus, Massachusetts, USA) and anaesthesia was maintained using a gaseous mixture containing nitrous oxide, oxygen, carbogen and isoflurane (see table 1 for dosage). Paralysis was established and maintained using Vecuronium (NOR-CURON, Organon Australia Pty Ltd) administered intravenously (see table 1 for dosage). The animal's body temperature was maintained between 36 and 37 degrees using a servo controlled heating blanket. Silver electrodes were

inserted into the frontal cortex and needles were placed in the skin on either side of the rib-cage to monitor EEG and ECG during the experiment. The end-tidal CO₂ (between 3.6 and 3.8%), the airway pressure (10 mm/Hg) and core body temperature were also monitored during the experiment at regular intervals. Dosages of the various drugs used for the procedures detailed above are presented in Table 1.

Using a microdrill, craniotomy was performed over the location of the primary visual cortex (V1) in macaques, and V1 and/or superior colliculus in tree shrews (SC; see table 1 for Horsley-Clarke co-ordinates). A durotomy was performed to remove the duramater, which both allowed a clear view of cortical surface for optical imaging as well as preserved the tip of the electrodes during microelectrode recordings.

The eyes of the animal were kept covered during surgery to protect the optics of the eye. Following surgery, the pupils were dilated using atropine sulphate (ATROPT 1%, Sigma Pharmaceutical Pty Ltd, Australia) and rigid gas permeable contact lenses, matched for the curvature of the eyes, were fitted to prevent corneal drying. In the macaques and earlier tree shrew experiments, the eyes were refracted using a hand held projectoscope and corrective lenses were placed in front of the eye during the experiment. In the macaques, an artificial pupil (diameter= 4mm) was also placed in front of the eye. In later tree shrew experiments (9 animals), refraction was also performed during the experiment by showing animals sine-wave gratings of increasing spatial frequencies. The power of the lens where the spatial fre-

quency resolution was the highest, was deemed the appropriate power. In most cases, the appropriate power was close to, if not the same as when no corrective lenses were added. As a result, corrective lenses were not used when they were not required, in order to limit any optical distortions the lenses may cause.

Once recordings were completed, the experiment was terminated by administering the animal a lethal dose of pentobarbital sodium (200-300 mg, Merial Australia Pty Ltd) intravenously. The animals were then perfused intracardially using phosphate buffer solution (PB; 0.1M), the brain was fixed using a paraformaldehyde solution (PFA; 4% Paraformaldehyde in 0.1M PB). The brain was removed and stored in a solution of 25% sucrose (0.1M PB) for cryoprotection. The brain was later processed for histology.

4.3 Electrophysiological Recordings

Single and multi-microelectrode recordings were made from the primary visual cortex (V1) and the superior colliculus of the tree shrews, and the macaque primary visual cortex as follows.

4.3.1 Single Electrode Recordings

A chamber was built around the opening using dental cement. Tungsten micro-electrodes (between 4 and 18 M; FHC, Inc., ME, USA) were inserted into the cortex and the well was filled with with Agar solution (2% Agar

in 0.9% Saline) for stability of recordings and protecting the cortex. The signal obtained from the microelectrode was first amplified (x 10,000 times; A-M Systems, WA, USA). An anti-aliasing filter (5000 Hz; A-M Systems) was applied to the signal and a HumBug noise eliminator (A-M Systems) was used to reduce 50 Hz line noise. Usually, this raw signal was further filtered between 300 and 3000 Hz and the signal was digitised at 22.5 kHz using an analog to digital converter (Cambridge Electronic Design Limited, Cambridge, UK). In some cases, the raw signal was also digitised in a separate channel for further analysis. The signal was also fed through an audio speaker and receptive field locations of the neurons were first plotted using the auditory feedback. The data was recorded and a template of the spikes was built using the Spike 2 software (CED, Cambridge, UK). Post stimulus time histograms (PSTHs) were built from the templated spikes for online analysis and the original signal was also saved for further analysis. At the end of each microelectrode track, electrolytic lesions were made by passing 6 A of current for 6 to 7 seconds to identify the locations of the recordings.

4.3.2 Multielectrode Recordings

A 16 channel multi-electrode array (individual electrodes spaced 100 microns apart; Neuronexus Technologies, Ann Arbor, USA) was used to record from the macaque V1. The array was connected to a pre-amplifier (RA16PA, Tucker-Davis Technologies, USA), via a headstage (RA16CH), where the signal was amplified (x 10,000) and filtered (2.2 Hz to 7.5 kHz) and digitized

at 12.5 kHz using TDTs OpenEx software suite. Further digital filters were applied to separate the signal into an LFP stream (2.2-100 Hz) and a multi-unit stream (300-3000 Hz). These were saved for further analysis.

4.4 Stimuli

Stimuli were presented on a BARCO monitor (Frame rate= 80 Hz; Reference Calibrator Plus; Barco Video and Communications, Belgium). All stimuli were generated using the stimulus description language (SDL) and presented using the ViSaGe stimulus generator (VSG; Visage, Cambridge Research Systems, UK). To assess the stimulus preferred orientation of a unit, moving bars of 9 different orientations (18 directions) were presented to the neuron. The eye that gave the weaker or no response was occluded. Width of the bar was usually set as the narrowest bar that could still elicit a good response. The length, polarity, contrast and speed of the moving bar were all customized to elicit the best response from the neuron. Once the orientation of the stimulus was determined, the animal was presented with sine-wave gratings to determine the spatial frequency tuning of the neuron. To obtain the spatial frequency tuning, the contrast and size of the gratings were optimised and the spatial frequency was varied in steps of 0.1 and 0.3 cycles/ $^{\circ}$. This was repeated at four different orientations 45 $^{\circ}$ apart.

4.5 Data Analysis

All single unit and multi-unit recordings were templated using the Spike 2 software to isolate neurons. Each neuron at the recording site usually has a distinct set of spike parameters (shape, duration and amplitude of the components) and the spikes that were similar (with at least 60% overlap) were grouped together as spikes from the same neuron. For each stimulus condition, a stimulus marker was produced and exported to the spike 2 software. The spikes from a neuron and the stimulus markers for each stimulus presentation were exported to a text file and analysed using custom software in MATLAB (The Mathworks Inc, MA, USA).

The spikes that followed the same stimulus were gathered and displayed in a post stimulus time histogram (PSTH) so that each PSTH displays the response of the neuron to one stimulus (eg: the response to a bar of a certain orientation). In order to build a PSTH, the spikes were grouped in 20 ms intervals and the number of spikes in each bin was divided by the bin width (in seconds) to get the firing rate of the neurons (in spikes per second or Hz). The PSTH was then convolved with a Gaussian kernel ($= 3$ bins) to get the stimulus density function (SDF, see Figure 1 for example) to account for the variation in the trial-by-trial firing rate. Further measurements were performed on the SDF to define the response of the neurons to various stimuli.

The response of the neuron to bars and gratings were quantified in different ways. For a moving bar, neurons showed a peak response when the

bar passed over their receptive fields. Figure 4.1 is the SDF of a neuron to a moving bar. As the bar moves over the receptive field, a peak is observed in the SDF (one for each direction). The response of the neuron is then the maximum response at each of the peaks (shown by the red circles).

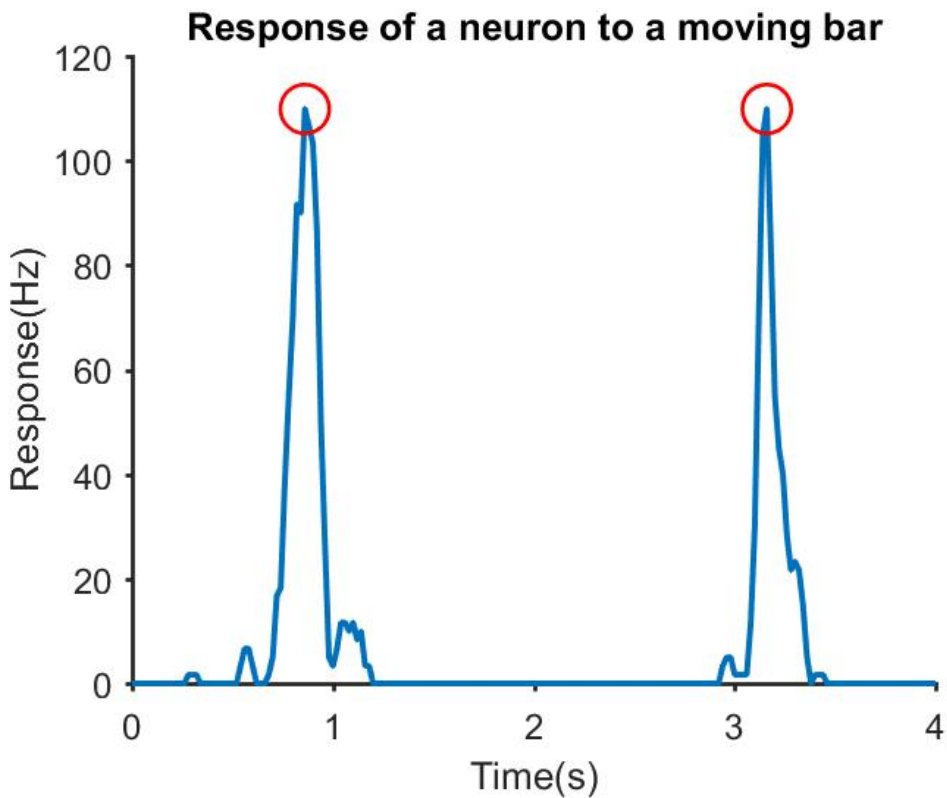


Figure 4.1: The SDF of a neurons response to a vertical bar moving bidirectionally. The maximum response in each direction is highlighted with red circles

When shown gratings, neurons respond differently. A neuron, based on whether it demonstrates linear summation over its receptive field or not,

responds differently to a grating. For example, linear cells give a response modulated to the temporal frequency of a grating (see Figure 4.2a; TF= 4Hz). A Fast Fourier Transform of the SDF is taken (Figure 4.2b) and the peaks observed indicate that the respective frequencies have a high magnitude in the original signal. In this case, the FFT has two distinct peaks (red circles), the first one is at 0 Hz and the second one at 4Hz. The peak at 0 Hz is the F0 component of the response and is equal to the average of the signal in figure 4.2a. The second peak is the F1 component and gives the fundamental frequency of the neurons modulated response (4 Hz). Non-linear cells dont show a modulated response to gratings, especially for higher spatial frequency gratings and as a result, the only distinct peak in the FFT corresponds to the F0 component (0 Hz).

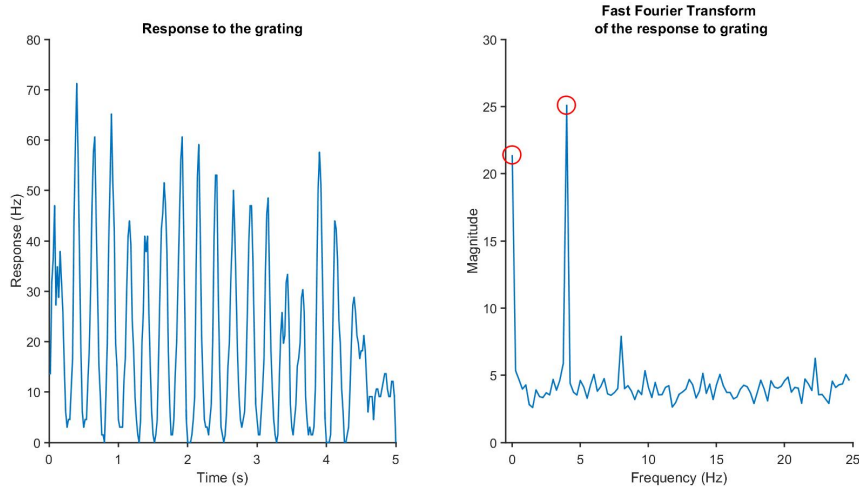


Figure 4.2: a) the SDF of a linear cell. The first 4.3s was the stimulus presentation duration. A blank screen was presented for the last 0.7s. b) The fast fourier transform (FFT) of the signal in fig4.2a. There is a peak at the F0 component as well as at 4 Hz, which was also the temporal frequency of the sine wave grating.

Cells were first classified as linear or non-linear neurons with our cortical and collicular data, comparable to the classical categories of simple and complex in the primary visual cortex (Hubel and Wiesel , 1962) and X and Y like in the lateral geniculate nucleus (Enroth-Cugell and Robson, 1966). This was done by taking the modulation index (Skottun et al., 1991) which is the ratio of the F0 and F1 components of the response. Traditionally, the modulation index is calculated by dividing the F1 component of the response by the F0 component. Neurons with modulation index less than 1 were classified as non-linear cells and cells with modulation index greater than 1.5 were clas-

sified as linear cells. Recently, a modified measure of the modulation index was proposed to measure linearity in the tree shrew primary visual cortex (Van Hooser et al., 2013). Using this measure, the range of values the modulation index could take was between 0 and 2 where neurons with modulation index less than 1 were classified as non-linear cells and where neurons with modulation ratio between 1 and 2 were classified as linear cells. This measure of modulation index was chosen to enable comparison with earlier tree shrew studies. For non-linear cells, the F0 component of the response was used for further analysis while for linear cells, the F1 component was used. From the response of the neuron to drifting sinusoidal gratings of increasing spatial frequencies, the spatial frequency tuning curves of the neuron was constructed and the peak spatial frequency and the half width at half height were calculated.

4.6 Histology

After the experiment, the tissue was processed for histology as follows. The brain was stored in a 25% sucrose solution until it sank. This was to ensure that the tissue was cryoprotected. The brain was cut into blocks so that only the areas of interest were sectioned. The brain was frozen and 50 micron sections were made using a cryostat (Leica CM3050S, Leica Microsystems, Nussloch, Germany). The sections were collected and stored in a Sodium Azide solution (0.1% in 0.1M PB) till they could be mounted on gelatinised

slides after which they were dried overnight and stained.

4.6.1 Cresyl violet staining

First the sections were dehydrated using increasing concentrations of ethanol solution. Then, chloroform was used to de-fatten the sections. This was followed by rehydrating sections in decreasing concentrations of ethanol. The sections were then stained using Cresyl Violet Acetate solution (0.1%, Sigma-Aldrich, Inc., USA) and differentiated using a solution of 5% percent acetic acid in 95% ethanol. The sections were then fixed in histolene and the slides were coverslipped.

4.6.2 Track Reconstruction

In order to reconstruct electrode tracks, the electrolytic lesions were located under a light microscope and digitised (Zeiss Axiocam Digital Camera, Zeiss, Germany). The shrinkage was calculated by comparing the recorded and observed distances between lesions using Adobe Illustrator(Adobe systems software Ltd). The shrinkage calculation was used to accurately determine the actual depth of the units recorded. In tree shrew V1, based on the location of the unit, it was classified as layer 4 or layer 2/3. In the shrew superior colliculus, the units were categorized as either belonging to the superficial or deeper layers of the superior colliculus.

4.7 Optical Imaging of Intrinsic Signals

Optical imaging of intrinsic signal is a high resolution imaging method that is used to detect the changes in blood oxygenation level in areas of neuronal activity. As a result of neuronal activity there is increased oxygen consumption in the surrounding tissue which leads to an increase in the level of de-oxy haemoglobin in the blood. This leads to a difference in reflectance in the tissue between regions where there is oxygenated and de-oxygenated blood and it is this signal that OI detects. This is the same signal as the fMRI BOLD signal but optical imaging has one key advantage over BOLD imaging. Whereas the fMRI signal has the resolution in the scale of millimetres, OI can detect signals at at least one order of magnitude higher resolution, allowing us to visualize the organization of neuronal activity at the scale of cortical columns. So, Optical imaging was used to image the functional activity of the macaque primary visual cortex.

4.7.1 The apparatus

In order to acquire OI maps of the primary visual cortex, first, a tandem lens macroscope was attached to a slow-scanning CCD camera. A light source is used to provide illumination for the duration of the imaging and the acquired frames were converted into a digital signal using an analog to digital converter. The specifications of these equipments are detailed below.

Macroscope and camera

A tandem lens macroscope was constructed by arranging two camera lenses (Pentax lenses, $f= 50\text{mm}$) end-to-end. This macroscope had a shallow depth of field which allowed us to focus at a specific depth below the surface of the cortex. In this manner, we acquired the blood flow changes related to the neuronal activity at the depth where the lens was focused. The macroscope was connected to a slow scan CCD camera (Teli CS 8310B; Tso et al., 1990) which acquired and transmitted images to the imaging system (VDAQ Imager 3001, Optical Imaging, Rochester, NY).

The Chamber

As the images were acquired in-vivo in an anaesthetized macaque, there was the possibility of the image being contaminated by movement artefacts caused by the animals respiration and heartbeat. To reduce this, a metal chamber (diameter= 10 mm) was placed on the skull surrounding the exposed cortical area. It was sealed in place using dental cement (Dentimex VA, Netherlands) and ensured that no leaks were present. Once the chamber was fixed to the skull, it was filled with Silicone oil (Polydimethylsiloxane 200 fluid, viscosity 50 cSt, Sigma-Aldrich, Inc., USA) and sealed with a coverslip. In the macaque, due to the angle of the imaged area, we used a metal chamber without the metal pipes traditionally used to fill the chamber. The cylinder was overfilled with Silicone oil and the coverslip tightened. Where bubbles were present, the process was repeated until a clear view of the cortex was

achieved.

The Illumination System

A circular fibre-optic attachment was connected to the camera lens for uniform illumination during optical imaging. First, a green light filter (545 nm) was used to obtain an image of the cortical surface with blood vessel landmarks (the green image). Then a longer wavelength (630 nm) filter was used for imaging. This wavelength of light was used because it was shown to reliably isolate the haemodynamic changes related to neuronal activity. Shorter wavelength lights (≤ 600 nm) reveal more of the blood volume changes while light of wavelength longer than 630 nm primarily detected light scatter effects. Light at 630 nm was the longest wavelength of light we could use to ensure maximum penetration of the light into the cortex while still imaging the haemodynamic changes.

4.7.2 Image acquisition

Stimulus presentation

Stimulus was generated by the ViSaGe system and displayed on the BARCO monitor as described below. The Visage and the camera were synchronized by the means of an optical imaging interface (VDAQ Imager 3001, Optical Imaging, Rochester, NY). The interface started the camera when the stimulus presentation began. The stimuli were eight full field, bidirectional, square

wave gratings (contrast =100%; Spatial Frequency = 1-2.5 cycles/degree; Temporal Frequency = 1.5 Hz) of changing orientations. The stimulus was presented for 7.2 seconds, followed by a 10 second blank. This inter-stimulus interval allowed the OI signal to return to baseline. This was repeated 50 times to improve the signal-to-noise ratio.

Image acquisition system

The macroscope was focused below the surface of the cortex between 550 and 700 m. Then, when the stimulus was presented, the Imager 3001 simultaneously started the camera which acquired 18 frames, each 400 ms long while the stimulus was presented. There was no image acquisition during the inter stimulus blank time. In order to get an image of the cortex at rest, a blank stimulus was presented for 7.2 s, followed by a 10 s interstimulus interval. The camera had a 14-bit bit-depth, which allowed the detection of very small variations in the OI signal. The individual frames for each block (10 trials per block) were first saved by the imaging system and exported to MATLAB for further analysis.

4.7.3 Analysis of Intrinsic Signals

Pre-processing of the data

Prior to the analysis, the data acquired had to be corrected for luminance artefacts. We did this by averaging frame numbers 3 to 16 from all the 50

trials for each stimulus condition (between 1200 and 6800 ms) and dividing it by the average of the first frame across 50 trials. These frames were chosen as the signal from OI when using the 630 nm light is biphasic (see figure 4.3). The initial signal first dips below the baseline and then increases later, peaking at approximately 5 s after the stimulus was presented. This is generally consistent with the time-course of the de-oxyhaemoglobin concentration (Malonek and Grinvald, 1996). To account for the illumination effects, the first frame subtraction method was employed to create a differential map. In this method, the blank was taken as the first frame and the activity of all other frames are calculated as the difference of the frame from the blank frame. This division by the blank is equivalent to subtracting and dividing by the blank since the optical imaging signal is relatively small (see Pouratian & Toga, 2002).

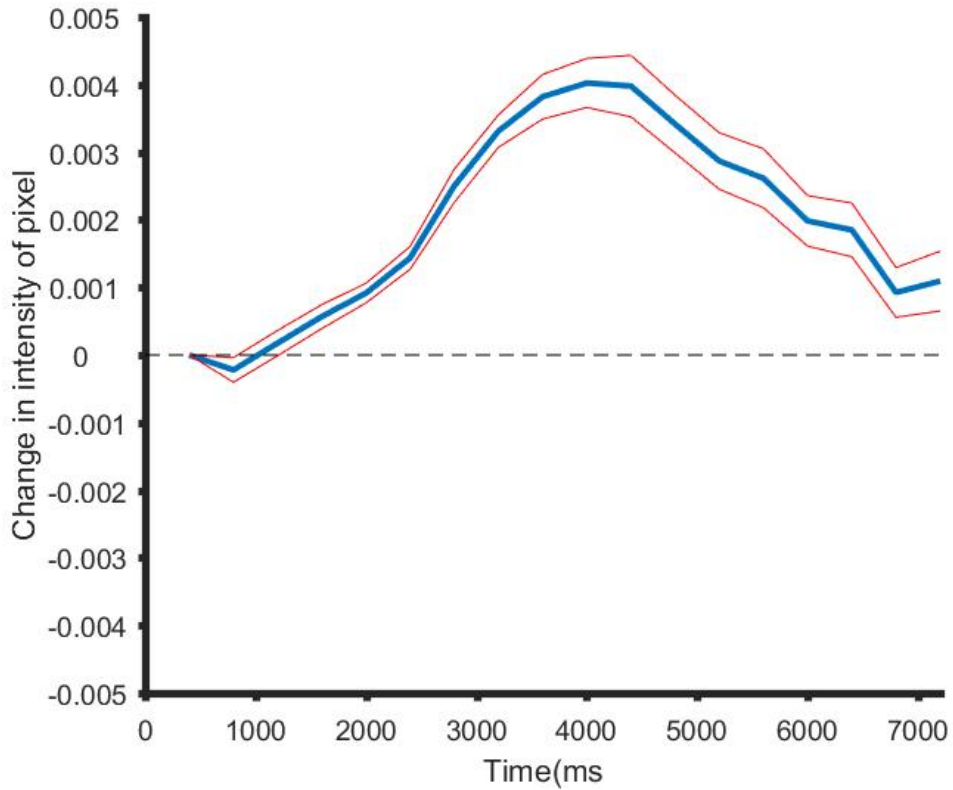


Figure 4.3: The time course of the OI haemodynamic signal for the duration of the stimulus presentation. The deoxyhaemoglobin levels briefly increase before decreasing, leading to a decrease in pixel intensity followed by an increase.

Obtaining single condition and orientation maps

The differential map is bandpass filtered in order to obtain the single condition map. This is done as follows. First the differential map is low pass filtered using a Gaussian kernel with a large sigma value (312.5 microns).

The low pass filtered map is subtracted from the differential map to obtain the highpass filtered map which is once again filled with a Gaussian kernel with a small sigma value (100 microns). The resulting map is the single condition map (SCM; see figure 4).

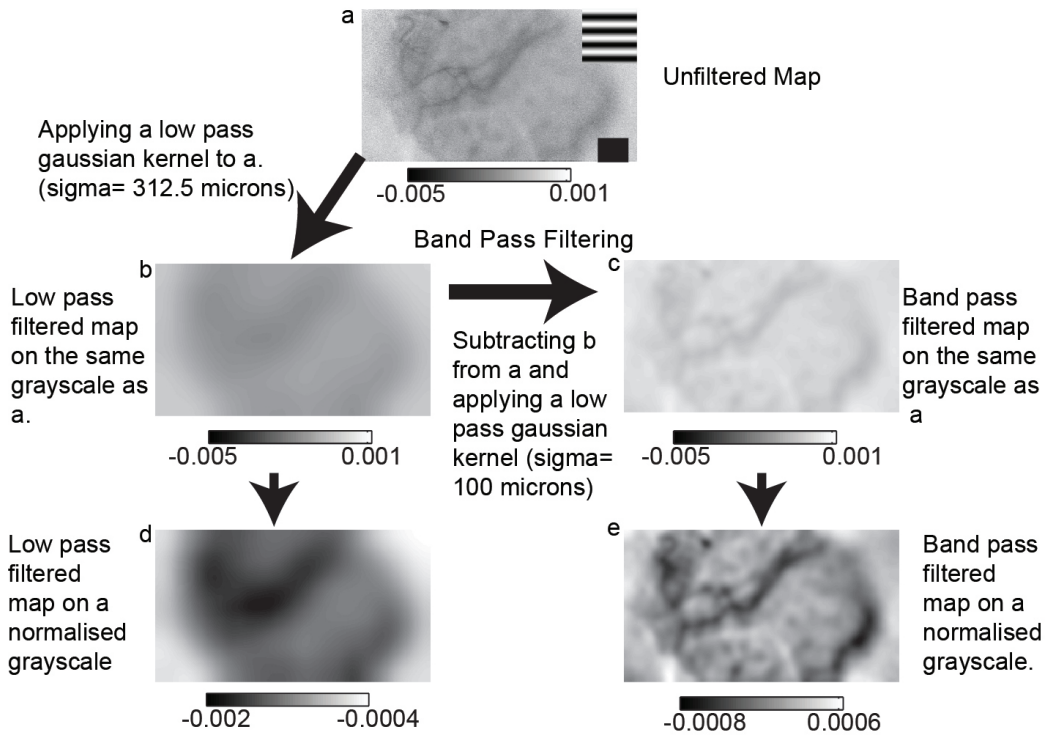


Figure 4.4: The filtering process used to generate single condition maps. The differential maps are first high-pass filtered to remove spatial scale signals and a smaller low-pass, smoothing filter was used to remove the high spatial noise.

The single condition maps obtained for each orientation are then vector averaged (Swindale, 1998) to create the orientation domain map.

Chapter 5

**Radial Bias in large spatial
scale optical imaging signal in
the macaque Primary Visual
Cortex**

5.1 Summary

Neurons in the primary visual cortex are tuned to orientation and similarly oriented neurons are arranged in columns, with orientation columns arranged like spokes around a pinwheel. The different orientations are however not equally represented. Two different types of biases have been reported in the representation of orientations in the primary visual cortex, namely the oblique effect and the radial orientation bias. Electrophysiological and fMRI studies have shown a preponderance of the radial orientation in the primary visual cortex of mammals. However, optical imaging of intrinsic signals (OI), which are related to the fMRI signals do not show this radial bias. Here, OI signals on a spatial scale comparable to that of the fMRI signals were examined. The orientation selectivity of the spatially unfiltered, raw signal obtained from OI was compared to the radial angle and a significant radial bias was found in this signal. When a similar analysis was performed on a traditionally band-pass filtered OI signal, a much weaker radial bias was found. As the OI signal is predominantly due to synaptic and pre-synaptic activity, it is proposed that the global signal in OI corresponds to cortical inputs. If the cortical inputs are biased for only a small number of orientations, then this provides evidence for a model of orientation selectivity where orientation tuning of cortical neurons are sculpted from orientation biases encoded in a small number of broadly tuned channels.

5.2 Introduction

Neurons in the primary visual cortex are tuned to orientation and the orientation tuned neurons are organised in columns. Hubel and Wiesel (1962) showed that neurons in Area 17 of cats were sharply tuned to orientation. These neurons were also grouped into neurons of similar orientation. Optical imaging studies in the cat A17 and 18 showed that the cortical orientation columns were organised as the spokes of a pinwheel, converging on the pinwheel centre (Bonhoeffer and Grinvald, 1991; Grinvald et al., 1986). Models of orientation selectivity and cortical architecture assume that neurons are equally tuned to all line orientations. However, studies suggest that there is an overrepresentation of some orientations in the visual system. Two types of orientation biases have been demonstrated in the visual system. The first is the oblique effect, which manifests as an underrepresentation of the oblique orientations while the horizontal and vertical orientations are overrepresented (see Appelle, 1972 for review). The second is the radial bias; where neurons are preferentially tuned to the orientation parallel to the line joining the centre of the receptive field to the centre of the visual field (Levick and Thibos, 1980). Both these biases have been reported in the macaques.

Where the relationship between the receptive field location and visual field locus were studied, a radial bias has been reported every time. Early studies of biases in orientation representation in the cortex reported a strong oblique effect in electrophysiological studies (Chapman and Bonhoeffer, 1998;

Coppola et al., 1998; DeValois et al., 1982; Kennedy et al., 1985; Leventhal, 1983; Li et al., 2003; Mansfield, 1974; Mansfield and Ronner, 1978; Orban and Kennedy, 1981, Payne and Berman, 1983; Pettigrew et al., 1968); which was congruent to the findings of a prominent oblique effect in behavioural studies reported in most species, from humans to octopuses (Appelle, 1972; Campbell et al., 1966; Furmanski and Engel, 2000; Rovamo et al., 1982). However, these studies examined the orientation preferences of neurons without studying their corresponding receptive field locations. Later studies that characterised the receptive field location with regards to the visual field locus all reported a radial bias in almost all species that were studied using electrophysiological studies (Levick and Thibos, 1980; Levick and Thibos, 1982; Maloney et al., 2014; Passaglia et al., 2003; Leventhal, 1983; Leventhal and Schall, 1983; Smith et al., 1990; Vidyasagar and Henry, 1990; Schall et al., 1986a; Schall et al., 1986b, Shou and Leventhal, 1989), fMRI imaging studies (Sasaki et al., 2006; Swisher et al., 2010; Mannion et al., 2010) and behavioural studies where subjects observed natural scenes instead of oriented gratings (Hanson and Essock, 2004).

One of the key tools that have been instrumental in revealing cortical architecture is optical imaging of intrinsic signals (OI). Using OI, not only have the ocular dominance domains and orientation domains been visualised, but their relationships with each other have also been examined (Bartfeld and Grinvald, 1992). The haemodynamic change accompanying neural activity that is recorded using OI is akin to the BOLD (Blood Oxygen Level Depen-

dent) response observed in fMRI (Menon et al., 1995; Logothetis et al., 2001). While the orientation biases studied using the fMRI BOLD responses reveal a radial orientation bias, only the oblique effect has been reported using OI (Chapman and Bonhoeffer, 1998; Coppola et al., 1998; Grabska-Barwinska et al., 2009).

One reason for this discrepancy in these findings could be due to the spatial scale at which these signals are studied. The BOLD signal has a poorer spatial resolution compared to the OI signals, which is capable of resolving cortical columns (Churchland and Sejnowksi, 1988). The BOLD and OI responses predominantly consist of the pre-synaptic and synaptic activity with the extracellular, spiking activity forming a fairly small part of the response (Logothetis et al., 2001). Traditionally, images obtained using OI are band-pass filtered to reflect activity corresponding to a narrow spatial scale (between 100-500 microns). While this spatial filtering has the advantage of isolating the weaker, smaller spatial scale spiking activity, it has the disadvantage that by omitting the larger spatial scale activity, any information present at this spatial scale is lost. Here, we aimed to use the unfiltered larger spatial scale signal. We hypothesised that when this larger spatial scale signal is studied in the anaesthetised macaque striate cortex, we will find a bias for the radial orientation as has been reported in the fMRI studies.

5.3 Methods

In this study, we imaged and recorded from the cortex of five, anaesthetised male macaques (*Macaca nemestrina*, 2-4 years old). All experimental procedures were approved by the Florey Institute of Neuroscience and Mental Health Animal ethics committee and conformed to the guidelines of the National Health and Medical Research Councils Australian Code of Practice for the Care and Use of Animals for Scientific purposes.

Surgery and anaesthesia

Surgical procedures were as described in the methods section. Briefly, animals were anaesthetised using a Ketamine/Xylazine mixture (Ketamil, 15mg/kg, i.m., Parnell Laboratories, Australia; Cylazil, 2mg/kg, i.m., Troy Laboratories, Australia). Venous cannulation was performed on the cephalic vein to administer fluids and paralysant (Norcuron, initial bolus of 0.7 mg/kg followed by 0.2 mg/kg/hr, Organon Australia Pty Ltd) to the animal and a tracheostomy was performed to administer the anaesthesia (0.5-2% Isoflurane in a mixture of nitrous oxide and oxygen (70:30)) during the experiment. The animal was placed in a stereotaxic frame and its head fixed using ear bars. During the experiment, the end-tidal CO₂ (3.6-3.8%), electrocardiogram, electroencephalogram and the core body temperature were all monitored. A craniotomy and durotomy were conducted over the location of the primary visual cortex (Horsley-Clarke co-ordinates: 24-34 mm posterior and 2-10mm

lateral). The eyes were dilated by applying 0.1% Atropine (Sigma Pharmaceuticals Pty Ltd, Australia) and rigid, gas permeable lens were introduced to prevent corneal drying and optical lenses and artificial pupil (4mm) were used to correct any refractive errors and reduce optical aberrations.

Optical Imaging of Intrinsic Signals

Setup Optical imaging of intrinsic signals was used to obtain the haemodynamic change related to the neural response to orientation stimuli. The OI setup involved two camera lenses (2 x Pentax lenses, $f=50$ mm) arranged in a tandem fashion (Frostig et al., 1990) connected to a CCD camera (Teli CS8310B). The tandem lens arrangement allowed us to choose a narrow plane of focus. An LED light source was used to illuminate the cortical surface. Before stimulus presentation, a high contrast, green image of the surface of the cortex was obtained by illuminating the cortical surface with a green light (filter wavelength=545 nm). This provided us with cortical landmarks which were later used in determining the locations for electrode tracks of topographical recordings. Following this, the camera was focussed between 550-700 microns beneath the surface of the cortex and a red light filter (wavelength =630 nm) was used to illuminate the cortex.

Stimulus and data collection During the experiment OI maps were obtained in response to visual stimulation. Visual stimulus was generated using the visual stimulus generator (SDL, Cambridge Research Systems, UK) and

presented on a Barco monitor (Reference Calibrator plus; Barco Video and Communications, Belgium). The monitor was positioned at 57 cm from the animal. The stimulus presented was a full field, square-wave, bidirectional, drifting grating ($SF = 1\text{-}4$ cpd, $TF = 1.5$ Hz, Contrast = 100%). The orientation of the grating changed sequentially in 22.5 degree steps from zero to 157.5 degrees. A zero degree grating was a horizontal grating moving bidirectionally. The stimulus was presented for 7.3 seconds followed by an interstimulus interval of 10 seconds where the animal viewed a blank screen. 18 frames, each 400 ms long were collected for each stimulus presentation. The signal to noise ratio was enhanced by acquiring data over 50 trials collected in 10 blocks of 5 trials each. Where possible, given the condition of the imaged area and the animal, the experiment was repeated for a second time. Using the OI data acquisition system, each block was exported as a MATLAB file. Each individual frame in a block was the average of that frame over 5 trials. Analysis was conducted on the exported MATLAB files.

Image Analysis Of the 18 frames collected, the mean of 14 frames (frames 3-16) was calculated for individual blocks in each stimulus condition. The first frame was then subtracted from the averaged frames for each stimulus condition. The mean of 10 blocks was then calculated. This gave us the unfiltered single condition maps (unfiltered SCMs). Traditionally, when analysing the images obtained using optical imaging of intrinsic signals, the unfiltered SCMs are band pass filtered using the method described in figure

(Refer to method figure). The unfiltered map is first low pass filtered using a large spatial filter (Gaussian filter, sigma= 312.5 microns). This removes the low frequency information. By subtracting this low pass image from the original image, we preserve only the high spatial frequency information (high-pass SCMs). The high pass SCM is then smoothed with a gaussian filter with a smaller sigma value (100 microns). This is the band pass filtered single condition map or more commonly just referred to as the single condition map (these will be referred to as filtered SCMs throughout this thesis). The filtered SCMs are then vector averaged to look at the angular mean of individual pixels (Swindale, 1988). This will produce the traditional filtered orientation tuning maps. In our study, we also vector averaged the unfiltered SCMs. We called the maps derived this way the unfiltered orientation maps.

Topographical recordings

High impedance tungsten microelectrodes (6-12 M Ω , FHC Inc, ME) were used to record from predetermined locations on the imaged cortical surface. The analog signal was amplified and filtered (AM Systems model 1800, Washington; Gain = x10,000; Band pass between 300 and 3000 Hz). The filtered signal was then visualised using an oscilloscope and fed through an audio speaker to aid in plotting the receptive fields. First the foveal location (if visible) and the optic nerve with blood vessel markers were plotted using a back-projecting fundus camera. Then the locations of the receptive fields were carefully hand plotted using handheld stimuli from at least 3 locations

in the imaged area. In between each electrode penetration, where possible, the location of the fovea and optic nerve head were replotted in order to account for eye movement. At six locations, the signal obtained from the electrodes and the filtered signals were digitized (12.5 - 22.5 kHz, CED; Cambridge Electronic Systems, UK) and stored for later analysis.

Multi-electrode array recordings

In one animal, we used a 16 channel, linear, multi-electrode array (NeuroNexus Technologies Inc, USA) to record from the cortex. The array was inserted at an angle within the supragranular layers of V1. The individual electrode on the multielectrode array were separated by 100 microns. The array was connected to a pre-amplifier (RA16PA, Tucker-Davis Technologies, USA) through a headstage (RA16AC). The signal was amplified (x 10000) and filtered (2.2 Hz- 7.5 kHz) was applied and the resultant signal was digitized (12.5kHz) using the OpenEx software (TDT, USA). The digitized signal was further digitally filtered between 2.2Hz and 100 Hz, and down-sampled to 1017.3 Hz to obtain the LFP signal and between 300-3000 Hz to obtain the multi-unit recordings.

Stimulus for electrode recordings

To make topographical recordings, a handheld stimulus was used. The orientation, direction and speed of the stimulus movement were all varied so that the neuron was ideally stimulated. Following this, the receptive fields

of the neurons were hand-plotted and used for further analysis.

For the single electrode recordings and linear array recordings, a bi-directional moving bar (10o x 0.5o bar, contrast = 100%, speed= 2.5- 5o/s), whose orientation changed incrementally from -90o in steps of 20o was used. The responses were recorded for 9 orientations with bars moving in 2 directions (a total of 18 directions) over 10 trials. The monitor used to present the stimuli and software used to generate the stimuli were the same as described for optical imaging.

Data Analysis

Analysis of electrophysiological recording For both the single electrode and the linear array recordings, multi-unit activity and LFPs were analysed to get the optimum orientation at a recording site. For recordings made using single electrodes, the Spike 2 software (Cambridge Electronic Systems, UK) and for linear array recordings, the Open Ex Software (TDT, USA) were used to apply digital filters to separate the signals into LFP (between 20 and 70 Hz) and multiunit activity (between 300-3000 Hz). The LFP signal corresponding to each stimulus direction was averaged across 10 trials using custom code written in MATLAB. The difference between the peak and the trough of LFP signal at each orientation, over the location of the receptive field, was the maximum response at this orientation. These values were used to generate the polar plots and calculate the circular mean (as calculated by Swindale, 1998; See Appendix for code) at each of the recording

sites. For multi-unit activity, a threshold was placed using the spike 2 software and any spike the was greater than this signal was collected into PSTHs and SDFs were made. The peak firing rate at each direction of movement was used to generate polar plots and calculate the circular mean of the data.

Determining radial orientation- receptive field locations In order to determine the azimuth and elevation of receptive fields obtained during the experiment, the Cartesian co-ordinates of the foveal location was set as (0,0). The horizontal and vertical distances of the receptive field centre from the foveal location were calculated. The azimuth and elevation of receptive fields were then calculated as the horizontal and vertical angles subtended by the animals eyes to the receptive field centre. If there were eye movements during the experiment, (0,0) was re-assigned to the new foveal location. Receptive field locations were replotted in relation to foveal locations plotted closest to the recording in order to get as accurate a receptive field location as possible. This then allowed us to accurately determine the azimuth and elevation of the receptive fields.

Using the receptive field locations thus calculated, we used the eccentricity, azimuth and elevation values to calculate iso-azimuthal and iso-elevation lines on the cortex. We used previously published magnification factor calculations in the macaque cortex (Dow et al.,1981) to calculate the magnification factor degrees in visual space one would traverse if we moved 1 mm in cortical space and the inverse magnification factor; how far one needs to move on

the cortex to traverse 1 degree in visual space, given the eccentricity of the receptive fields. These values were used to calculate the azimuth and elevation of points on the cortex that were spaced 15 pixels (375 microns) apart. The radial angle of each of the points was calculated given the azimuth and elevation of their RF locations and averaged to calculate the average radial angle of the imaged area.

Defining a region of interest As described above, the azimuth and elevation of points on the cortex that were 375 microns were calculated. 30 x 30 pixel squares around these points were defined as Regions of interest (ROIs). The difference between the average optimum orientation of the individual pixels in the ROIs and the radial angle of the ROI centre was calculated for both the unfiltered and filtered orientation maps (See fig5.1).

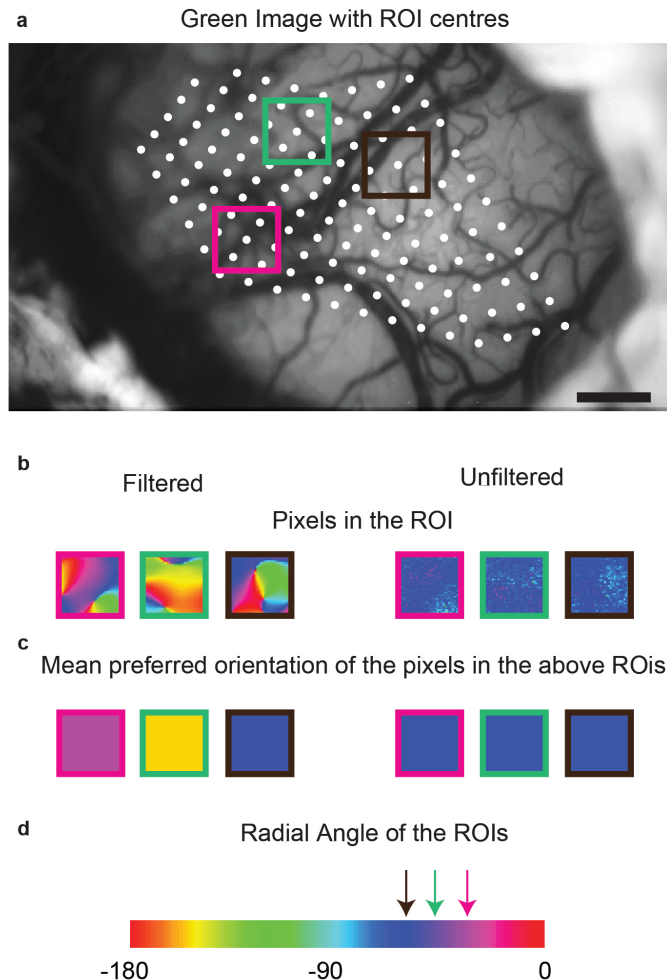


Figure 5.1: The generation of Regions of Interest (ROIs). a) the green image from the representative animal. The white dots are the centres of the ROIs. The ROIs were placed 15 pixels apart. Three ROI centres were randomly chosen and the region that is used for analysis is shown by the three coloured squares. b) shows the individual pixels in the filtered and the unfiltered conditions in the respective ROIs. c) shows the average orientation of the pixels in the ROIs. d) is the pseudo-color scale used to represent the different orientations in the orientation tuning maps and the pixels in the ROI. The three coloured arrows indicate the radial angle of the corresponding ROIs.

Single Pixel Analysis The ROI analysis was used to determine if any of the cortical inputs were dominant in the larger spatial scale. To see if such bias was present at a single pixel level, we also compared the orientation tuning of single pixels to the radial bias of the imaged area. Accordingly, the optimum orientation of the individual pixels was subtracted from the mean radial orientation of the imaged area for the unfiltered and filtered maps.

Adjusting for sample size in single pixel analysis During the single pixel analysis, individual pixels from orientation maps in five animals were examined. This amounted to a large number of pixels (10^5 pixels). In order to make sure we were not detecting an insignificant effect made significant by sample size, we randomly resampled with replacement from the distribution of pixels in both the filtered and the unfiltered conditions to see if an effect could be observed at smaller sample sizes. We used two sample sizes (40 and 1000) sampled 1000 times and calculated the chi-square of the 1000 trials. The mean and the 95% confidence intervals of the chi-square value from 1000 trials were calculated. If the upper limit of the 95% CI of the chi-square value was lower than the 5% critical value, then the distribution of the single pixel differences was not significantly different from a uniform distribution in the majority of trials. If the lower limit of the 95% CI was higher than the 5% critical value, then the distribution of the single pixel differences was deemed significantly different from a uniform distribution in the majority of trials.

5.4 Results

We recorded from 5 monkeys (*Macaca fascicularis*, all male, aged between 2 and 5 years). In 3 monkeys, we imaged and recorded from the left hemisphere and in the other 2, from the right hemisphere. In all animals, OI signals were first recorded from the respective hemisphere; following this, topographical recordings were made. In 2 macaques, LFP recordings were made using single electrodes and in one macaque, the multi-electrode, linear array was used for recordings.

Single Condition Maps

As a first step in processing the results of OI, SCMs were made. The SCMs for the unfiltered and filtered maps from one representative animal are presented in figure 2a and b respectively. The orientation of the stimulus is shown above the respective SCM. The SCMs show that there is more activity overall in orientations closer to the radial orientations (denoted by the star) in the unfiltered maps (i.e. the overall map is darker). No such trend is visible in the filtered maps. Distribution of the intensities of the pixels of inverted SCMs (So that darker pixels have a greater intensity value) are presented in figure 2c. The line above the boxplots indicates the range of radial orientations of the imaged area in this animal. As observed in the SCMs, there is a peak at the radial orientation in the unfiltered maps while the distribution of the filtered pixels show no such trend.

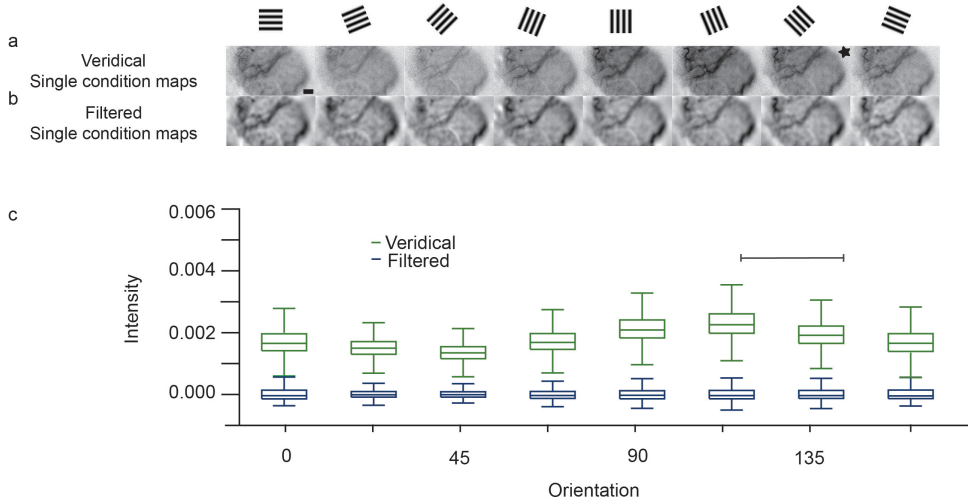


Figure 5.2: Distribution of pixels in unfiltered and filtered SCMs. (a) and (b) are the unfiltered and filtered SCMs. The stimulus orientation corresponding with each SCM is presented in the row above. The star denotes the orientation closest to the radial angle. Scale bar is 1mm. (c) is the boxplot of the distribution of the intensity of pixels in the unfiltered and the filtered maps. The line indicates the range of radial angles in the imaged area.

Orientation Tuning Maps

The unfiltered and filtered SCMs shown in figure 2a and b were vector averaged (Swindale, 1998) to produce the unfiltered and the filtered orientation maps in fig.5.3. Figure 5.3a is the green image of the cortical surface with surface blood vessel landmarks. The different symbols correspond to the location of electrode tracks. The receptive field locations of the electrode tracks are shown in figure 5.3b. The polar plot corresponds to the orientation of a

layer 2/3 neuron recorded from the location indicated by the diamond. The orientation of this neuron estimated using electrophysiological recording was 65.61° ; which was less than 22.5° away from the orientation of the neuron estimated using optical imaging was 86.89° . The pseudo colour scale on the outside of the Cartesian scale is the same scale used in parts c and d. Figure 5.3c shows the filtered orientation maps and Figure 5.3d, the unfiltered orientation maps obtained during two repeats of the experiment. The filtered orientation map shows classical orientation domains that converge at a pinwheel centre, while the unfiltered orientation map is dominated by one orientation. This orientation corresponds to the radial orientation of the receptive fields in figure 5.3b; i.e. if we draw a line from the center of fixation to the center of the receptive field and extend it to the outer colour scale, we will observe the same colour as that seen in the unfiltered maps. Results for the unfiltered maps are presented in a similar fashion for all the animals in our study in figure 4.

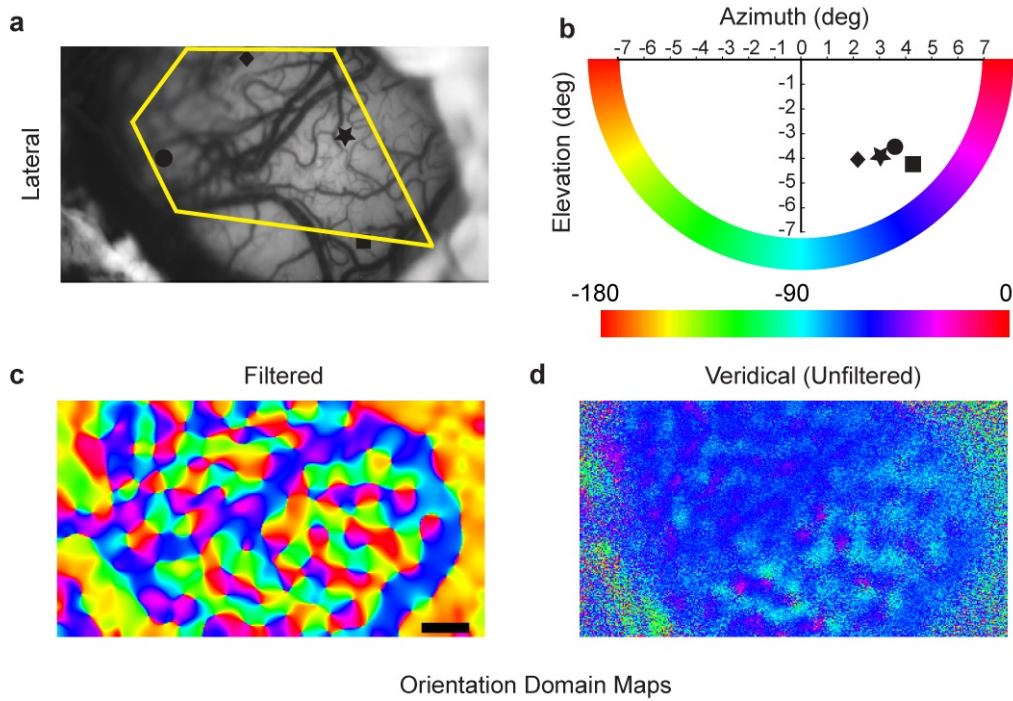


Figure 5.3: Orientation tuning of the filtered and unfiltered signals. a) the cortical green image showing the cortical landmarks and the location of the electrode tracks. b) the different symbols indicate the receptive field location of the respective electrode tracks. The polar plot indicates the orientation of the unit obtained using single unit recording. The outer pseudo-color scale is the same as the one used in c and d. c) and d) are the filtered and the unfiltered maps.

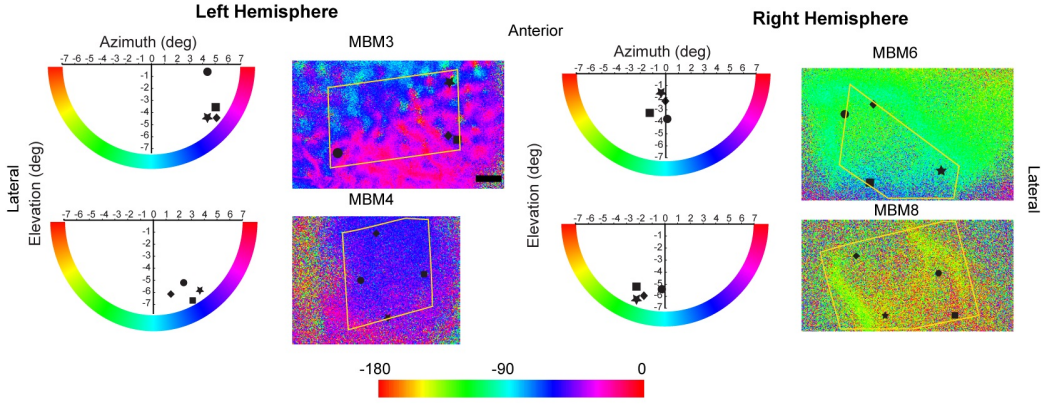


Figure 5.4: The receptive field location, veridical and filtered orientation tuning maps of all the animals (except that showed in figure 5.3) used in our studies. The conventions are as explained figure 5.3.

Comparing the radial orientation and optimum orientation of ROIs

The optimum orientation of the pixels in the ROI and the radial angles of the ROIs were calculated and compared as described in the methods for 456 ROIs. Most ROIs were tuned to the radial orientation in the unfiltered maps. In the filtered maps, this bias for the radial orientation in the ROIs was observed to a smaller extent. Figure 5.5a shows the distribution of the absolute differences between the optimum and radial orientations of the ROIs for the unfiltered and filtered orientation maps. The distribution of differences was significantly different from a uniform distribution for the unfiltered ($\chi^2 = 505.28$; $df=3$; $p<0.0001$) as well as the filtered conditions ($\chi^2 = 35.21$; $df=3$; $p<0.0001$). The filtered and the unfiltered distributions were

also significantly different from each other ($\chi^2 = 283.01$; df=3; p<0.0001).

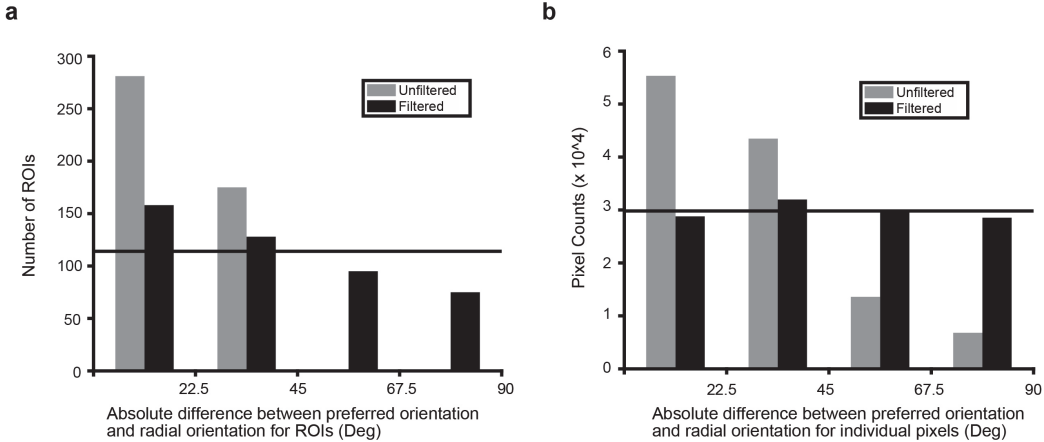


Figure 5.5: a) The absolute difference between the optimum orientation and the corresponding radial angle of the ROIs. Horizontal line is the distribution we would expect if the distribution was uniform. Total number of ROIs= 456. b) The distribution of absolute differences between the optimum orientation of single pixels and the radial angle of the imaged area.

Comparing the radial orientation and optimum orientation of single pixels

The ROIs average the signal over 900 pixels (30X30 pixel square). We also examined the difference between the optimum orientation of individual pixels and the mean radial orientation of the imaged area to see if the radial bias was also present at the single pixel level. The single pixel differences showed that most pixels in the unfiltered condition were tuned to the radial orientation. Figure 6 shows the distribution of differences between the

individual pixels and the mean radial orientation for the unfiltered and the filtered conditions. Once again, there was a strong peak between 0 and 22.5 degrees in the unfiltered condition. When compared with a uniform distribution (indicated by the horizontal line); the distribution of the differences for the unfiltered condition was significantly different ($n= 119229$; $\chi^2= 54691$; $df=3$; $p<0.0001$). No clear anisotropies were observed in the filtered single pixel responses although the overall response was still significantly different from a uniform distribution ($n= 119229$; $\chi^2= 246.24$; $df=3$; $p<0.0001$). The distribution of the filtered differences were also significantly different from the unfiltered differences ($n=119229$; $\chi^2= 54077$; $df=3$; $p<0.0001$). We did not find any significant biases for horizontal and vertical orientations in either the ROI or the single pixel data.

For the single pixel analysis, as we used a large sample size (119229), the chi-square test, will always give a significant result regardless of the effect size. In order to address this issue, we used a repeated sampling paradigm, where smaller samples were randomly chosen from the overall pixel population and chi-square tests were performed on these distributions. We used two sample sizes (either 40 or 1000) and sampled 1000 times (1000 trials) from the overall population. The results indicate that the radial bias observed in the unfiltered maps were strong and were observed even in the condition with a relatively small sample size of 40 pixels (mean $\chi^2= 21.09$; CI= [20.95, 21.24]; χ^2 critical =7.05). There was also a statistically significant radial bias observed with the larger sample size of 1000 pixels for the unfiltered maps

(mean $\chi^2 = 461.93$; CI= [461.68, 462.19]; χ^2 critical =7.05). For the filtered maps however, while the distribution was significantly different from a uniform distribution when sample size was 119229, the distribution was not significantly different from a uniform distribution when the sample size was 40 (mean $\chi^2 = 2.99$; CI= [2.84, 3.13]; χ^2 critical =7.05) or 1000 (mean $\chi^2 = 5.18$; CI= [4.92, 5.44]; χ^2 critical =7.05). These results suggest that the statistically significant result shown for a sample size of 119229 was most likely due to the large sample size. A summary of these results are presented in figures 5.6 and 5.7 for the 40 and 1000 pixel samples respectively.

40 pixels sampled 1000 times

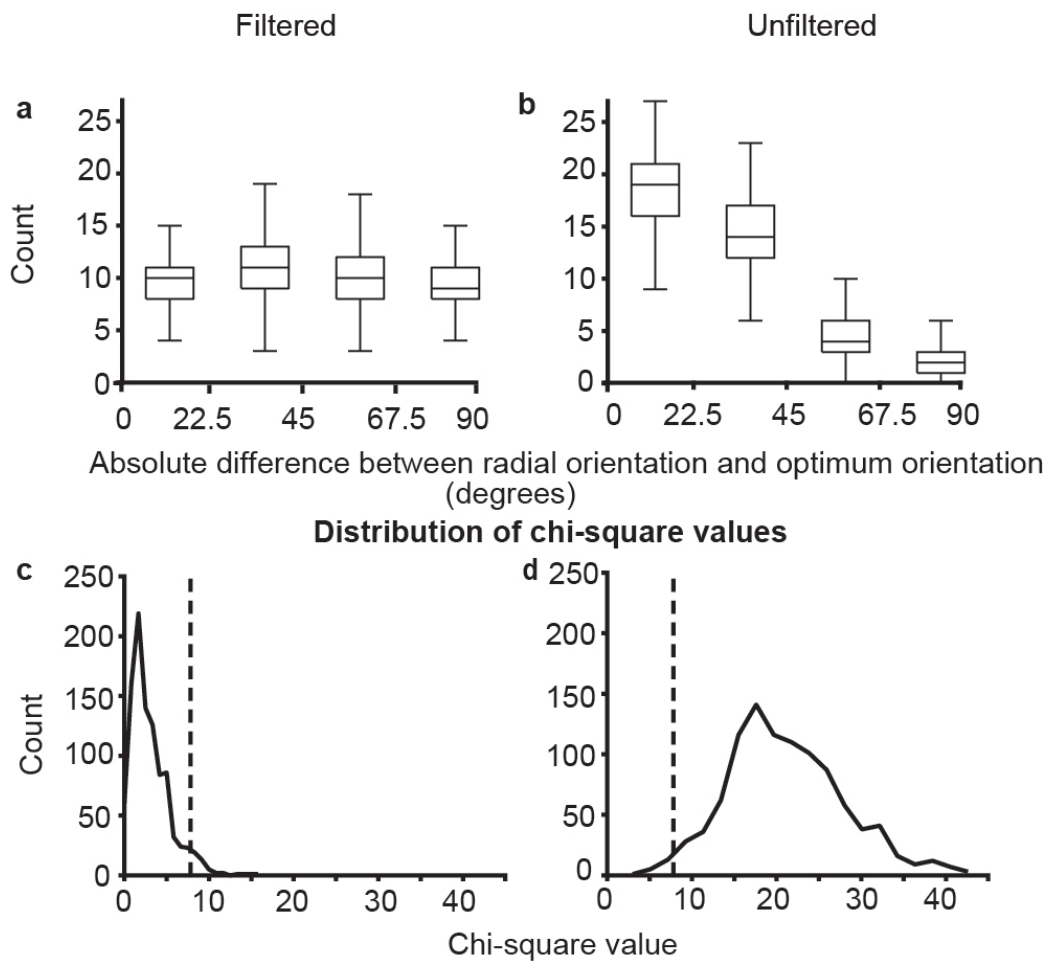


Figure 5.6: Results of the random simulation experiment with 40 pixels sampled 1000 times. a) and b) show the distribution of the preferred orientation of the single pixels, centered on the radial orientation in the filtered and unfiltered conditions respectively. The boxplot indicates the distribution of the values over 1000 trials. c) and d) show the distribution of 2 values for 1000 trials. The dotted lines indicate the location of the critical value for $p=0.05$.

1000 pixels sampled 1000 times

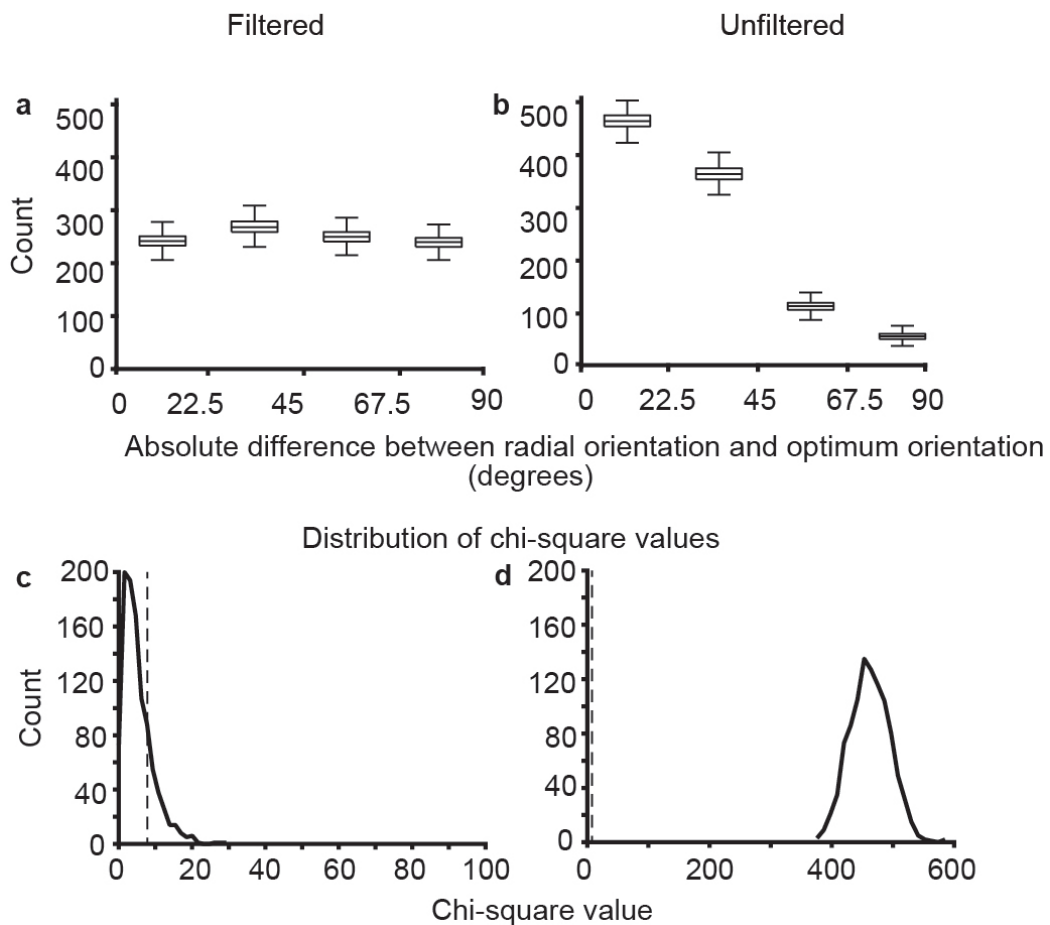


Figure 5.7: Results of the random simulation experiment with 1000 pixels sampled 1000 times. See figure 6 for description of individual panels

Orientation biases of the local field potentials

In two animals, we used single electrodes to record LFP as well as MUA from 6 recording sites. In one animal we used a multi-electrode array to

record the LFP and MUA at a further 16 locations. The orientation tuning of the MUA and LFP of the array data are presented in figure 8. The multiunit activity changed consistently across subsequent electrodes so that most orientations were represented. The LFP activity on the other hand showed broader orientation tuning. Further, most sites were tuned to the radial orientation. The absolute differences between the optimum orientation of the LFP and the multiunit activity, and the radial angle of the imaged area are shown in figure 5.8 . This includes all 22 sites (from single electrodes and multi electrode arrays). A chi-squared test showed that the distribution of the differences of circular means of the LFP was significantly different from a uniform distribution ($n=22$; $\chi^2= 8.18$; $df=3$; $p=0.04$) whereas the same was not true for the multi-unit activity ($n=22$; $\chi^2= 3.09$; $df=3$; $p=0.38$).

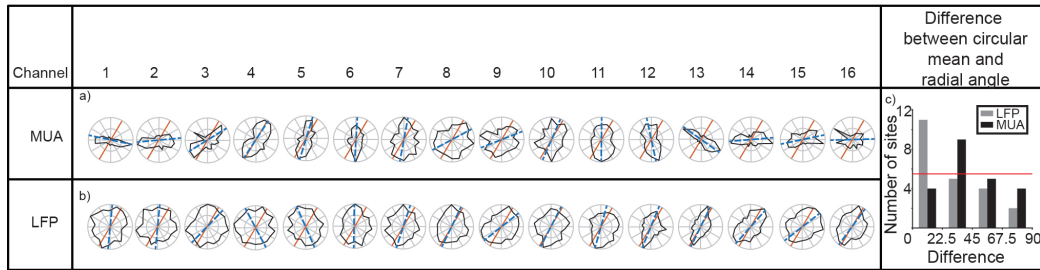


Figure 5.8: Results of the random simulation experiment with 1000 pixels sampled 1000 times. See figure 6 for description of individual panels

5.5 Discussion

Using optical imaging of intrinsic signals, we examined the OI signals at different spatial scales in the primary visual cortex of macaques. In a subset of animals, we also measured multi-unit responses and local field potentials in the primary visual cortex. We found that the large spatial scale signals in the OI and the LFP signals were tuned to the radial orientation while the smaller spatial scale signal and the multiunit responses did not show this preference for the radial angle. These results are consistent with the results from fMRI studies, where the BOLD signal is analogous to the OI haemodynamic signal, as well as the electrophysiological studies which show that in most animals studied, a radial bias exists in the visual system.

During the experiment, we could have introduced systematic errors in various stages of data collection and analysis. The plotting of the foveal location is dependent on the visibility of the fovea when observed through the fundus camera. The visibility of the fovea itself is dependent on the optics which tend to deteriorate as the experiment progresses. During the experiment, we were able to more accurately characterise the optic nerve head. As a result, both the optic nerve and the first foveal position needed to be accurately plotted for us to accurately determine the radial angle. An error in plotting either of these parameters could lead to inaccurate estimation of the radial angle.

Receptive field estimation is also subject to error. Within a track, there

is a jitter of approximately half a degree in both receptive field position and size of the receptive field (Dow et al., 1981). Further, we also only used the receptive field position of the first unit encountered in each track. This was to make sure that the angle of the electrode to the surface did not affect the measurement of receptive field location. This compared with the fact that the ROI centres are extrapolated from the RF measurements could introduce another element of error in our radial angle estimates. The formula used for extrapolation, though standardised, may not be exactly accurate in every animal. Large variances in topography between individual animals (eg: See Dow et al., 1981) have been reported in macaques which could further compound the error in radial angle estimates.

Further, the single pixel optimum orientations were all compared to the mean radial angle of the imaged area. The radial angles of the receptive fields in the imaged area can vary up to 30 degrees depending on the eccentricity of the receptive fields in the imaged area. This introduces a further element of error in the measurements which contribute to a larger spread of differences in the single pixel data. Taking into account all these sources of error in determining the difference between the radial angle and optimum orientation, the actual radial bias in the data may be stronger than has been reported.

In our study, we have shown that the larger spatial scale activity is tuned to the radial orientation. However, the question of what these signals represent remains. The large spatial scale, global signal has been attributed to local blood flow and blood volume changes in the imaged area (Stetter et al.,

2000; Pouratian and Toga, 2002). However, studies have shown that blood flow is also affected by neuronal activity through glial cells (Atwell et al., 2010), indicating that the blood volume changes accompany neuronal activity. One explanation lies in the fact that the BOLD responses (and therefore OI signals) are correlated with the LFP responses (Logothetis et al., 2001). This relationship is also demonstrated in our study, where the LFP and the global OI signal were both predominantly tuned to the radial orientation. While the exact nature of the LFP signal is still not understood, general consensus is that this signal represents the synaptic, pre-synaptic and multi-unit observed in the recorded region of cortex and does not correspond well with the multi-unit activity (Berens et al., 2008; Logothetis et al., 2001). We propose that the larger spatial scale, global signal also corresponds with the pre-synaptic, synaptic and multi-unit activity. By removing the higher magnitude, larger spatial scale signals using a band-pass filter, optical imaging studies help isolate the responses that correspond to the scale of the multiunit activity. Therefore, the large spatial scale signal in the OI response corresponds to the synaptic and pre-synaptic activity, which reflect the tuning of the inputs to the imaged area. Our results indicate that the inputs to the primary visual cortex are tuned to the radial orientation.

During imaging, the tandem lens arrangement allows us to focus on a very narrow plane under the surface of the cortex while imaging (Frostig et al., 1990). In this study, we focussed the tandem lens setup between 550-700 microns below the cortical surface. This depth corresponds to the region of

the cortex just above the interface between Layer 3 and Layer 4. Unlike the cat Area 17, most neurons in the macaque layer 4 show broad orientation tuning, with sharp orientation emerging in Layers 2 and 3 for the first time (Bullier and Henry, 1980). Further, the areas of layers 2 and 3 that were imaged also receive direct inputs from konio-cellular layers of the LGN (Klein et al., 2016). This indicates that the cells in the imaged layer, like their layer 4 counterparts show broad orientation selectivity. Therefore, despite the depth where the camera was focussed and images were obtained from, we can conclude that the inputs to the cortex are tuned to the radial orientation.

A previous study from our lab showed that inputs to neurons in the primary visual cortex were tuned to the same orientation as the orientation column to which they project (Vidyasagar et al., 2015). These results are not entirely contradictory to the results from our current study. Apart from any species differences that may be present, the earlier study showed a considerable jitter in the relationship between the orientation of the LGN fibres and cortical columns ($r= 0.63$). In our study, while the majority of the ROIs and pixels in the unfiltered maps were tuned to the radial angle, there were also a proportion that were tuned between 22.5 and 90 degrees away from the radial angle. This departure from the radial angle is similar to that shown in the earlier study (Vidyasagar et al., 2015).

If the inputs to the primary visual cortex are tuned to the radial orientation, then this has some implications for orientation selectivity in the primary visual cortex. The theory of excitatory convergence for the genera-

tion of orientation selectivity was first proposed by Hubel and Wiesel (1962) and proposed that thalamic neurons with circular receptive fields arranged in a row converged on a striate cortical neuron to endow on it sharp orientation selectivity. This model assumption that thalamic neurons are untuned to orientation. Contrary to this belief, many studies have shown that subcortical neurons are indeed biased for orientation (Hammond, 1974; Levick and Thibos, 1980; Vidyasagar and Urbas, 1982; Leventhal, 1983; Van Hooser et al., 2013; Vidyasagar and Henry, 1990; Smith et al., 1990; Passaglia et al., 2003; Shou and Leventhal, 1989; Sun et al., 2016). Our study adds to this extensive literature on sub-cortical biases by studying the organisation of the orientation selectivity of the inputs in the cortex, suggesting that most of these inputs are tuned to just one orientation. This provides support for a model of orientation selectivity where the inputs to the cortex arrive in a small number of broadly tuned orientation channels, from which the whole range of orientations observed in the primary visual cortex are generated (Vidyasagar and Eysel, 2015).

Vidyasagar and Eysel (2015) proposed that all orientations in the cortex can be generated by broadly tuned orientation channels with orthogonal orientations. However, our study only shows a bias for the radial angle in the inputs to the cortex. orientations. This does not necessarily mean that only one orientation is present in the inputs. The large magnitude of the radial bias signal could mean that any smaller signals maybe masked. There are no ways to separate these signals on a spatially (as is usually done in the

case of extracellular signals) without losing the information. Even if only one clear bias is present in the inputs, the cortex may still be able to generate all orientations. For example, phase selectivity is completely dominated by one polarity (75% of neurons respond to light off; Albus and Wolf, 1984) in kittens but the cortical networks generates both on and off neurons from these limited inputs (Xin et al., 2008). In colour vision too, normal colour vision can be achieved even though there are only a relatively small proportion of S cones and large variation in the proportion of L and M cones (Kremers et al., 2000).

Our study also highlights the importance of studying the optical imaging signal at different spatial scales as has been previously shown in cats, humans and macaques (Swisher et al., 2010; Tanigawa et al., 2017). In this study, we also highlight the use of optical imaging of intrinsic signals in studying the organisation of cortical inputs on a larger spatial scale. Future study can further characterise this large spatial scale, global signal which may be useful in determining organisation of inputs to the cortex.

5.6 Conclusion

In this chapter, we aimed to examine the large spatial scale activity in orientation maps to characterise radial bias in the optical imaging signal. We compared the optimum orientations of single pixels and ROIs to their radial angles and found that in the unfiltered maps, there was a prominent bias for the radial angle. The ROIs in the filtered maps showed a weaker bias for the radial orientation but no such bias was observed in the single pixel responses. We propose that these signals reflect the orientation tuning of the inputs to the cortex. If the majority of the inputs to the cortex are indeed tuned to the radial angle, then this provides evidence for a model of orientation selectivity where orientation input arriving in a small number of broadly tuned channels are further sharpened in the primary visual cortex to generate the whole range of orientation preferences observed in the cortex.

Chapter 6

Orientation tuning in the Tree

Shrew superior colliculus

6.1 Abstract

Though theories of orientation selectivity suggest that orientation biases observed in V1 inputs are the result of excitatory convergence, studies have shown that bias in the inputs may be inherited from neurons in sub-cortical structures, especially the retina and the lateral geniculate nucleus (LGN). Congruent with this theory, retinal and LGN neurons have been shown to be tuned to orientation at higher spatial frequencies. If orientation selectivity arises from the retina, it should be evident in other targets of retinal projections. The superior colliculus (SC) is one such area. Here, I examined the orientation selectivity of SC neurons in tree shrews using thin bars and gratings of various spatial frequencies. I found that SC neurons show orientation tuning comparable to that observed in layer 4 of V1 in the tree shrews and orientation biases reported in the retina and the LGN of cats and macaques. This orientation selectivity was more evident at higher spatial frequencies. These results indicate that orientation tuning observed in the inputs to the cortex maybe generated from the orientation biases present in earlier visual areas.(Swisher et al., 2010)

6.2 Introduction

The theory of excitatory convergence (Hubel & Wiesel, 1962) suggests that orientation tuning in the primary visual cortex (V1) is derived from inputs from circular lateral geniculate nucleus (LGN) neurons that are arranged in a row converging on the V1 neuron. While this theory has garnered a lot of support, it has also been widely contested. In this chapter, I aim to examine one of the main assumptions of this theory: that subcortical neurons are unoriented.

A long list of studies have shown that orientation biases are present in subcortical structures. Levick and Thibos (1980) initially showed that retinal ganglion cells were tuned to orientation at higher spatial frequencies. These results have since been replicated in both cats and macaques at the level of the retina and the LGN. The retinal orientation biases are set to be derived from the natural growth pattern of the retina which elongates the dendritic fields. Given that orientation tuning is only observed at higher spatial frequencies and the fact that V1 neurons only respond at higher spatial frequencies, the degree of orientation tuning observed in the inputs to V1 can be generated by a mere sharpening of biased inputs.

Intracortical recordings in cat V1 have shown that the EPSPs observed in cortical neurons are tuned to orientation. Ferster (1986) argued that this orientation tuning may be explained by excitatory convergence. However, Pei et al (1994) showed that when the dynamics of orientation selectivity were

examined, the earlier EPSPs showed broader orientation tuning, similar to that reported in the LGN and retina. These broader signals were further tuned by inhibition observed as IPSPs (Pei et al., 1994). Both excitatory convergence and retinal orientation biases can explain orientation tuning of cortical inputs. However, only retinal bias model is consistent with the degree of orientation tuning of the inputs and the dynamics of the PSPs.

If the retina were the seed of orientation selectivity in the visual system, we should be able to detect orientation bias in parts of the brain that also receive inputs from the retina. The superior colliculus, which forms an alternate pathway to the visual cortex receives direct inputs from the retina. The superior colliculus neurons in cats and macaques however, prominently show no orientation biases. Recent studies have somewhat redeemed the SC, with rodent SC neurons showing sharp orientation tuning (eg: Ahmadlou et al., 2015). While there seems to be a different model of orientation selectivity and cortical organisation in the rodent, I believe that SC neurons that receive direct retinal inputs will also be tuned to orientation. This is because orientation tuning in subcortical areas are only present at higher spatial frequencies and studies that looked for orientation tuning in the SC did not take this into account. Here I looked at orientation biases in the tree shrew superior colliculus.

The tree shrew was chosen for a few important reasons, foremost of which is that it has a large, distinctly laminated superior colliculus that has been well characterised. Studies showed that as in macaques and cats, the su-

peripheral layers of the shrew SC receives direct input from the retina and has been implicated in form discrimination. These layers are also part of an independent pathway to the extrastriate cortex which is essential in form perception. However, unlike cats and macaques, in the tree shrew superior colliculus, a previous study showed that a small proportion of neurons in the superficial layers of the shrew SC had distinctly elongated fields (Albano et al., 1978). This study might have missed any small orientation biases as only fields that were 3 or more times longer than they were wide were classified as orientation selective.

Here I examined orientation biases in the SC neurons in attempt to show that orientation tuning in the inputs to the cortex was a reflection of the bias observed in the retina. We hypothesised that orientation tuning will be revealed in the superior colliculus at higher spatial frequencies. In particular:

- a) When using thin, moving bars, the neurons will be tuned to orientation and;
- b) When tested using gratings of different spatial frequencies and orientation, orientation tuning will be evident at higher spatial frequencies.

6.3 Methods

6.3.1 Electrophysiology

The superior colliculus in the tree shrew is large and well laminated structure and runs from the posterior edge of the brain to AP 2 (Horsley & Clarke coordinates, Tigges & Shanta, 1930). Following surgery, a craniotomy was per-

formed over the location of the superior colliculus. High impedance, lacquer coated tungsten microelectrodes (FHC Metal Microelectrodes Inc., Bowdoinham, ME, USA; impedance= 12-18 M Ω) were lowered into the brain and the signal was amplified and filtered (x 10,000 gain, bandpass filtered between 300-3000 Hz, AM systems amplifier) and fed into an audio speaker as well as an analog to digital converter (CED, Cambridge Systems, digitised at 22.5 kHz). The SC was identified by listening to the neuronal activity in the speaker. The data was recorded as a spike trace using the Spike 2 software. The spikes were templated and the spike timing exported as a text file. Further analysis was performed using custom MATLAB code.

6.3.2 Stimuli

A hand held projectoscope was initially used to demarcate the receptive field boundaries. Using this, the centre of the monitor was aligned with centre of the receptive field prior to stimulus presentation. Stimuli was presented using a Barco Reference Calibrator Plus monitor (Barco monitor; Barco Industries, Belgium, Frame Refresh Rate= 100 Hz) and the stimuli were generated using Visage (VSG, Cambridge Research Systems, Cambridge, UK) and custom Stimulus Description Language (SDL) scripts. The monitor had a mean luminance of 32.6 cdm $^{-2}$. In some experiments, an antiglare, anti static screen was used. The luminance when this screen was used was 17.4 cdm $^{-2}$. The monitor calibration was regularly checked using the PR-650 spectrophotometer (Photo Research, Palo Alto, CA, USA). While recording,

the monitor was placed at a distance of 114 cm from the eye.

For each SC neuron, the preferred stimulus orientation was initially measured using a thin moving bar. The bar was presented in 9 different orientations sweeping bi-directionally (a total of 18 orientations.). The background was a uniform gray screen. Depending on the polarity of the neurons, either a bright bar or a dark bar was used (contrast= 100 %). The bar was on average 8° long (ranging between 4 and 8 degrees) and 0.5° wide (ranging between 0.1 and 1 degree). The velocity of the bar was between 5 and 20 $^{\circ}$ /second.

Peri-stimulus-time-histograms (PSTHs) were generated online using the spike 2 () software. Based on the PSTHs generated following the presentation of the bar, the optimum orientation of the bar was determined as the orientation that gave the maximum response. This orientation was used for further testing.

The spatial frequency response to gratings were then measured. The animals were presented with drifting sine-wave gratings of varying spatial frequencies (TF= 4Hz, SF= 0 cpd to 2 cpd) at 4 different orientations (optimum, optimum + 90° , optimum+ 45° , optimum- 45°). In some cases, responses to a complete orientation tuning stimulus (16 directions/ 8 orientations) were recorded in order to further quantify the orientation response at a certain spatial frequency.

6.3.3 Data Analysis

Regardless of the stimulus presented, the following analysis was performed on the extracellular trace before any specific analysis. Spikes were templated based on their polarity, size and timing and the spike time and stimulus marker exported into text files. Using custom scripts in MATLAB (see Appendix), peri-stimulus-time-histograms (PSTHs) were constructed for each of the stimulus conditions. Spike density functions were created using a 3 bin moving average function. This SDF was used for further analysis.

For orientation tuning recorded using a bar, the peak response in the SDF for each direction was plotted on a polar diagram. The circular mean of this maximum response and the corresponding direction was calculated using the following formula:

The circular variance (CV) and the orientation selectivity index(OSI) were also calculated as follows:

$$CV =$$

$$OSI =$$

For the gratings, the Discrete Fourier Transform (DFT) of the spike density function was calculated using the MATLAB fast fourier transform algorithm. The F1 and the F0 component were calculated as mentioned in the general methods. The F0:F1 ratio was calculated at the peak spatial frequency. The peak spatial frequency is the maximum spatial frequency after which both the F0 and the F1 decrease. If the F0 response was smaller than the F1 response (ie. the ratio was less than 1), the cell was deemed to be

X-like and the magnitude of the first harmonic component of the response was used for further analysis. If the ratio was greater than 1, the cell was considered non-linear and the F0 component was used.

The spatial frequency tuning at the optimum and orthogonal orientations were calculated by linearly interpolating between the data points. The bandwidth during which the superior colliculus neurons responded for the optimum orientation but not for the orthogonal orientation was calculated. In order to do this, a minimum response was first defined as the response rate at the spatial frequency where the response between the optimum and orthogonal orientations were no longer significantly different. The spatial frequency where the response rate for the optimum and orthogonal orientations first reach the minimum response was termed the optimum SF cutoff and orthogonal SF cutoff. The difference between SF cutoff for the optimum and orthogonal spatial frequencies were calculated.

6.4 Results

Anatomical location of units

A total of 22 units (5 tracks in 3 Tree Shrews) were recorded from. The laminar position of all the units were determined by reconstructing the electrode tracks using electrolytic lesions. The photomicrograph from one of the Nissl stained sections in one of the tree shrews is presented in figure 6.1a. In this section, lesions made in 2 separate tracks are visible (red arrow points to one

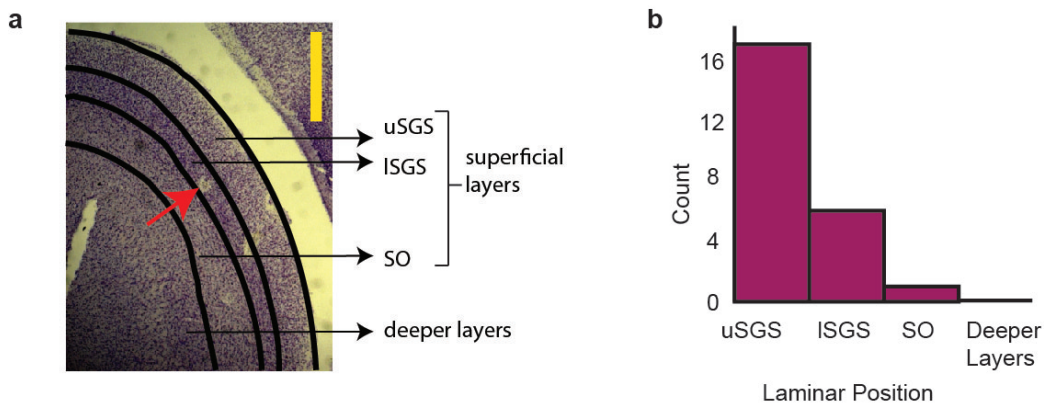


Figure 6.1: Histology. a) A section of tree shrew superior colliculus showing electrolytic lesions. Red arrow points to an electrolytic lesion. Scale bar (yellow vertical line) denotes 1000 m. b) A summary of laminar position of recorded units in the superior colliculus. Abbreviations: uSGS- upper Stratum Griseum Superficiale; ISGS- lower Stratum Griseum Superficiale; SO- Stratum Opticum.

of them). The different layers of the tree shrew SC are marked. The superficial layers are further distinguished. Electrode reconstruction was completed in all animals and the laminar position of each of the neurons is shown in Figure 6.1b. All the neurons we recorded from were located in the superficial layers with the majority being in the Stratum Griseum Superficiale (SGS) where the retinal inputs terminate.

Orientation Selectivity

The response of a representative neuron to moving bars of different orientations and the corresponding orientation tuning curves are presented in figure showed in figure 6.2. The response was the average of 10 trials and the small error bars suggest that the response was highly consistent (Error bars = \pm sem). The CV of this neurons was 0.82. The median CV of all the neurons in our sample was 0.82 with a range of [0.29, 0.94]. Any neuron with CV greater than 0.9 was considered not selective to orientation. Two neurons had a CV greater than 0.9 and were excluded from further analysis. The orientation tuning curves of the most selective, least selective neuron with Cv less than 0.9 and the least selective neuron in the entire sample are presented in figure 6.3. The histogram of all the circular variances are presented in figure 6.4.

Spatial Frequency Tuning

When the spatial frequency tuning response of the neuron at different orientations was observed, 13 of 16 neurons were orientation tuned at higher spatial frequencies. The spatial frequency response of an example neuron at the optimum and the orthogonal orientations is presented in figure 6.5a. The response is the F0 component of the FFT. The gray shaded area represents the spatial frequnecies where the neuron still responds to the optimum orientation but no longer responds to the orthogonal orientation (ie. the neuron is orientation tuned). The upper limit of the gray shaded area (the dotted line to the right) is the cut off spatial frequency at the optimum orientation.

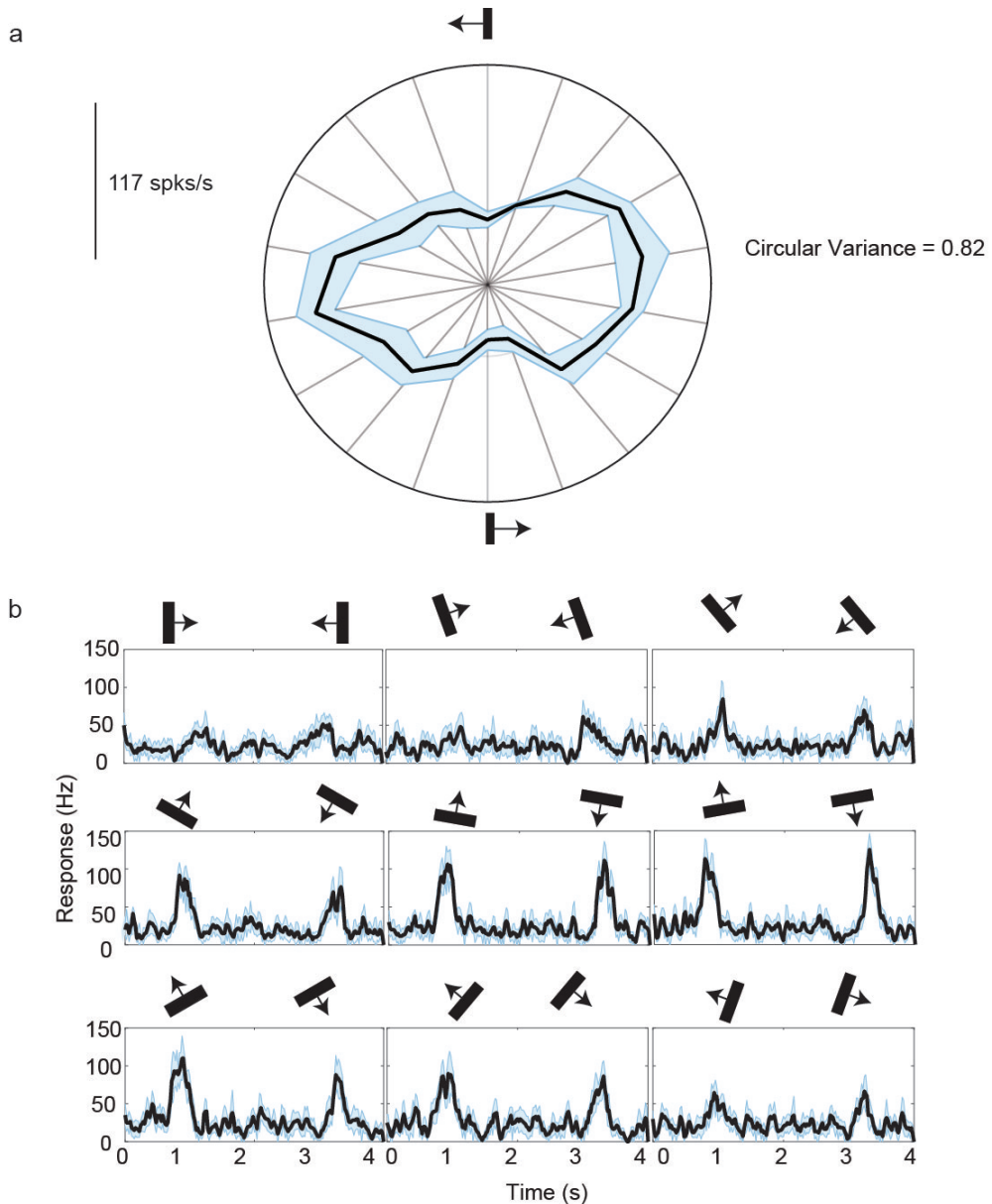


Figure 6.2: Orientation response of an example cell. a) The polar plot of the orientation responses of a neuron in the tree shrew superior colliculus. Each spoke represents an orientation presented. The circular variance of this neuron is 0.82. This was also our median circular variance. b) The spike density functions for different orientations for the neuron whose polar plot is shown in a. The orientation and direction of movement of the bar is shown above the trace.

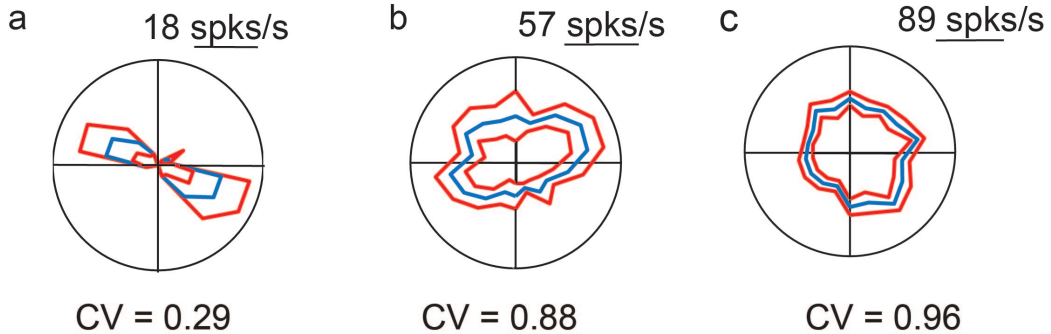


Figure 6.3: Polar plot showing the orientation tuning of the bar. Error bars denote Standard error. Orientation tuning curves of the sharpest (a) and the least tuned (b) neurons included in our analysis. (c) was the least tuned neuron in our sample

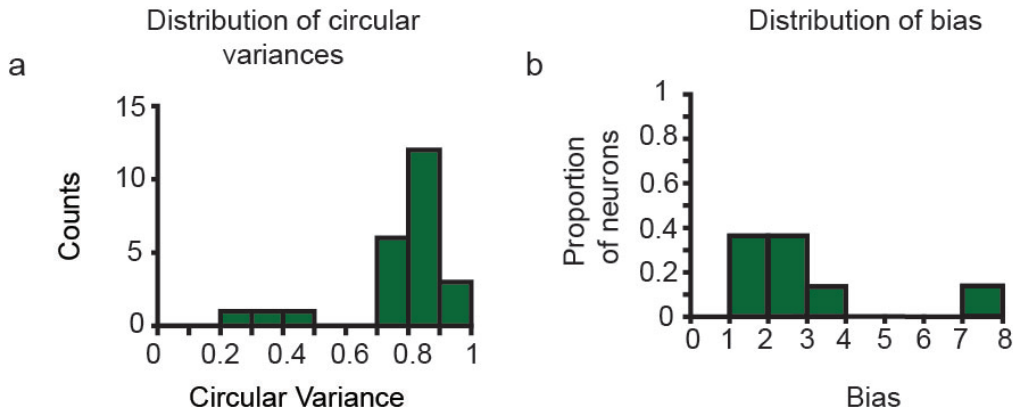


Figure 6.4: Circular variances: (a) This figure shows the distribution of circular variances of all neurons. Most of the tuned neurons have a CV between 0.7 and 0.9. The apparent second peak is discussed further in the discussion (b) This figure shows the laminar position of the individual neurons plotted against the circular variances. Apart from the three neurons in the upper SGS that are sharply tuned to orientation, there doesn't seem to be any differences in the orientation selectivity between the upper and lower SGS. There was an inadequate sample from the SO for comparison.

The sf corresponding to the lower limit of the shaded gray area is the cut off spatial frequency. The difference in response between the optimum and non-optimum orientation cut off frequencies was calculated. These results for the group are presented in figure 6.6 a. On average, the response to the orthogonal orientation reached the minimum 0.5 cpd before the response to the optimum orientation; with the 95 percent CI= [0.4, 0.6].

The OSI at each of the spatial frequencies for the example neuron is plotted in figure 6.5 b and the group results are presented in figure 6.6 b. The neuron exhibited the highest bias close to the cut off frequency at the orthogonal orientation.

6.5 Discussion

The results of this study demonstrate that neurons in the superior layers of the superior colliculus are tuned to orientation at higher spatial frequencies. This finding in combination with other reports of orientation biases in sub-cortical areas renders one of the key assumption of the excitatory convergence model that subcortical neurons have circular, unoriented receptive fields which then requires the arrangement of their receptive fields in a row to give rise to orientation tuning incorrect. Not only do tuned cortical inputs then pave the way for intracortical inhibition to sharpen orientation selectivity, they also abet the development of cortical architecture.

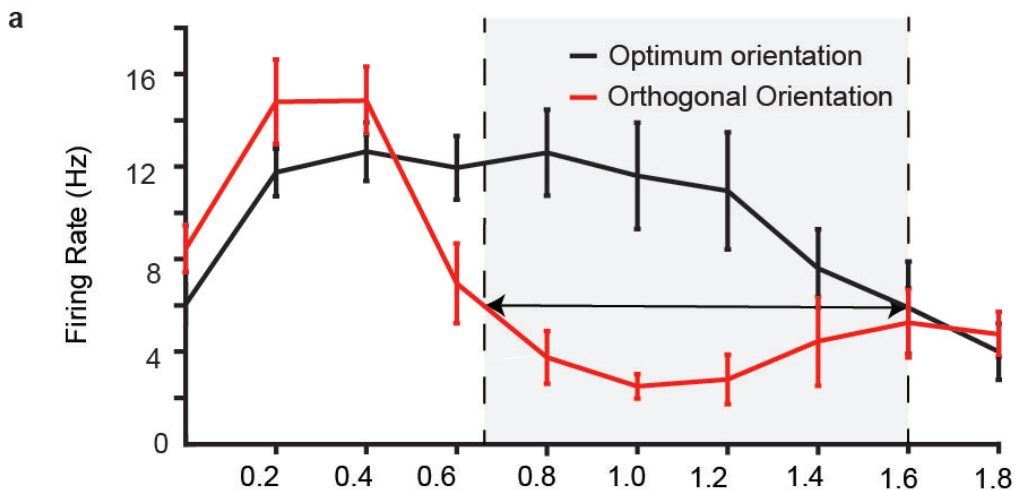


Figure 6.5: Example SF tuning curves for optimal and orthogonal orientations. The cut-off frequency at the optimal orientation is the SF at which the response at optimal orientation is no longer significantly different from the response at orthogonal orientation. The response at the cut-off frequency for optimum orientation is called the minimum response. For the orthogonal orientation, the cut-off frequency was the SF at which minimum response was first reached.

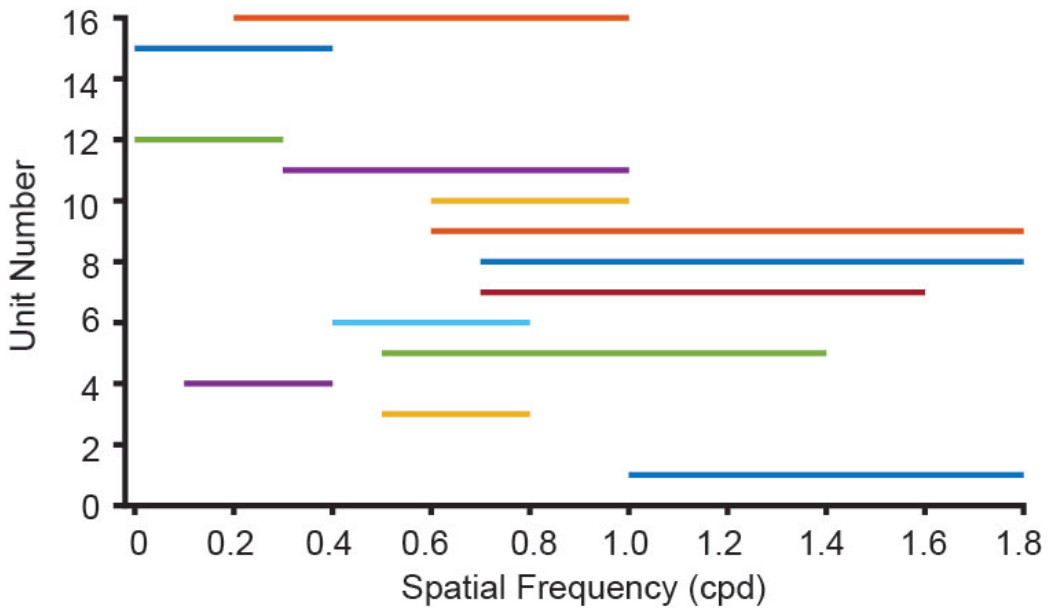


Figure 6.6: The difference between the cut-off frequencies for the optimum and orthogonal orientations for 16 units is shown in Figure 3b.

6.5.1 Anatomical Relevance

The histology confirmed that all the units that were recorded from the superficial layers of the superior colliculus. While the superior colliculus receives information from all the sensory modalities, the superficial layers receive direct input from the retina and feedback projections from the primary visual cortex. They also project to extrastriate visual areas. Lesion studies have shown that when the shrew SC is lesioned, form perception is affected. In Studies where the primary visual cortex of the tree shrew was ablated while keeping the SC and extra-striate visual areas intact showed that tree shrews could still consciously perceive form information further implicating the superficial layers of the shrew SC in playing an important role in perception.

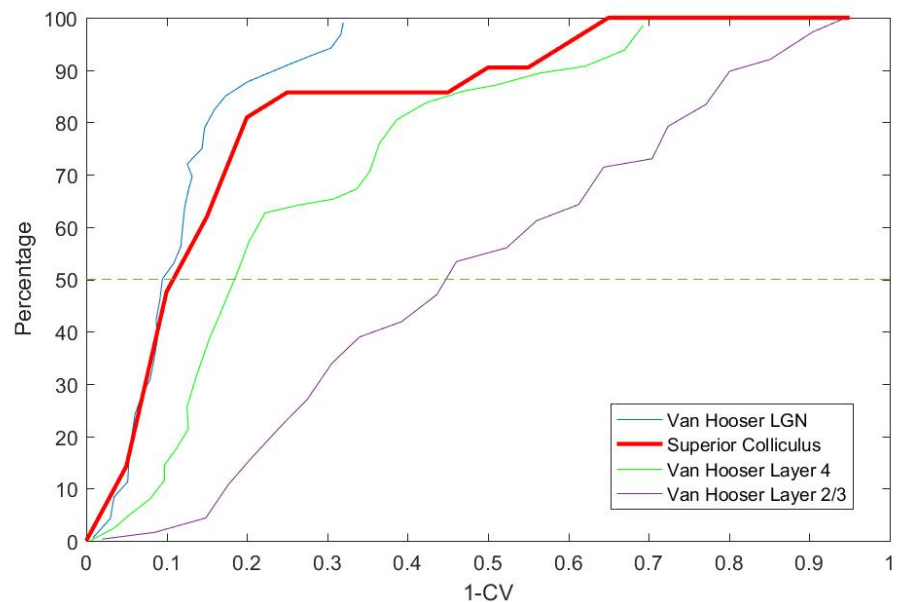


Figure 6.7: Comparison of the Superior Colliculus vs neurons in the geniculostriate system (data collected by Van Hooser et al., 2013)

Given its position in this alternate visual pathway and its role in form perception, it is surprising that orientation tuning has not been reported in the Superior Colliculus. Where it has been reported, like in the case of the tree shrews, a very small proportion of neurons have said to be tuned to orientation. These neurons have also been reported in the superficial areas of the superior colliculus.

6.5.2 Comparison with previous tree shrew studies

In their earlier paper, Albano et al., 1978 suggested that less than 10% of the neurons had elongated receptive fields. However, in our study, 90% of our neurons were orientation selective. It is important to make a distinction in these two results. While they may sound like it, these results are not entirely contradictory. In their study, Albano et al tested the elongation of the receptive fields. That is, using the neuronal responses, they plotted the receptive field boundaries of neurons and concluded that any neuron that had an aspect ratio of 3:1 had elongated receptive field. In this study on the other hand, we used the response of the neurons to bars and gratings of different orientations. Studies have shown that only a slight receptive field elongation is required for a neuron to give orientation specific response. Albano et al may have simply not detected smaller effects which have been reported in the retina and LGN due to their conservative criterion for classifying a neuron as orientation selective.

Another reason Albano et al., 1978 may not have detected the extent of

orientation tuning in the shrew SC could be the stimulus used. As mentioned earlier, bars and gratings were used in this study. Albano et al also used these stimuli however, only one paper was published (1974) in the cat retina indicating that orientation tuning was detected at higher spatial frequencies (Hammond, 1974). However, in the eighties, a lot of papers were published revealing the spatial frequency dependence of orientation tuning. The lack of this knowledge may also be one of the reasons why the orientation selectivity in the superior colliculus was missed.

Van Hooser et al., 2013 published a comprehensive set of data on the transformation of the receptive fields from the lateral geniculate nucleus to the layer 4 (input layer) to layer 2/3 of the tree shrew visual system. The orientation tuning of the superior colliculus neurons are plotted in relation to the geniculate, layer 4 and layer 2/3 neurons in the tree shrew in figure 6.7. This comparison indicates that the orientation biases observed in the superior colliculus are similar to those observed in the LGN of the tree shrew, with approximately 85% of the SC neurons having similar orientation tuning to the LGN neurons in the Van Hooser study. There is a tendency in our data for around 15% of neurons to have sharper orientation tuning than those exhibited in the LGN, closer to those seen in the cortex. While the neurons in the upper and lower SGS receive predominantly retinal inputs, there are also neurons which receive feedback projections from the primary visual cortex. These neurons could be one of the few neurons that receive cortical feedback. This can also be seen in figure 6.4 where the distribution

of circular variance seems to be in two different groups. However, the sample size in this study is too small to comment on this segregation.

6.5.3 Comparison with previous superior colliculus studies

The superior colliculus being a large, well laminated organ in most species was intensely studied for a while. The studies conducted in the superficial layers of the cat and macaque superior colliculus showed that the superior colliculus neurons were direction selective whereas no orientation selectivity was observed. In this sense, the SC was previously compared to the LGN both sub-cortical areas receiving unoriented input and relaying unoriented inputs to different pathways. However, the realisation that superior colliculus neurons may not be tuned to orientation at higher spatial frequencies seems to have not occurred in people who have investigated it. Recent rodent studies have shown that the rodent superior colliculus shows sharp orientation selectivity. Previous studies have demonstrated that the tree shrew superior colliculus is similar to the macaque visual system and the SC makes similar connections to extrastriate cortical areas in the macaque and the shrews. So it is possible that orientation biases are present in these animals as well and will be revealed when tested with higher spatial frequency stimuli.

6.5.4 Comparison with the geniculostriate system of cats and macaques

One of the prominent paper published investigating the spatial frequency dependence of orientation tuning in the retinal ganglion cells of cats was Levick and Thibos (1982). They characterised the way orientation tuning varied with spatial frequency. In the following paragraph, I will evaluate our results in the context of the responses of retinal ganglion cells.

One of the two key findings of Levick and Thibos was that RGCs were tuned to orientation at higher spatial frequencies. They also found that in some cases, at lower spatial frequencies, the neuron responded better at the orthogonal orientation compared to optimal orientation. They also reported that the degree of orientation selectivity (reported as orientation bias) was the maximum close to the threshold. In the tree shrew SC, all these findings hold true. A close examination of Fig: 6.5 shows that orientation tuning is observed at higher spatial frequencies. Figure 6.5 b also shows that the orientation bias was the maximum close to the threshold. Figure 6.6b also demonstrates this. Figure 6.5 is also only one example of a case where the neuron was biased for the orthogonal orientation at lower spatial frequencies. Neuron being oriented to different orientations at lower spatial frequencies was also a common finding in the superior colliculus. But the optimum orientation of the neuron as measured using bars was the orientation for which the SF cut-off was the highest in all cases. These properties have also

been more universally demonstrated in the retina of macaques and also the LGN of cats and macaques, further indicating that the orientation biases have a common, retinal ancestry.

6.5.5 Conclusion

In this chapter, I set out to examine if one of the key assumptions of the excitatory convergence model that subcortical neurons had circular receptive fields was indeed true. Previous studies in the retina and the lateral geniculate nuclei of cats and macaques have shown that subcortical neurons were tuned to orientation at higher spatial frequencies. I hypothesised that the tree shrew SC neurons would also be tuned to orientation at higher spatial frequencies. When examined with thin bars and gratings of increasing spatial frequencies, SC neurons were indeed tuned to orientation. These orientation tuned inputs may then be sharpened by intracortical inhibition to generate the sharp orientation selectivity we see in the primary visual cortex. Inputs tuned broadly to a small number of orientations could also give rise to the organisation of cortical columns. Finally, establishing orientation biases in the retina also reduces the functional redundancy of establishing orientation tuning in the different parallel pathways.

Chapter 7

**Is the tree shrew primary
visual cortex a linear filter?**

7.1 Summary

It has been contentious whether simple cells in the primary visual cortex (V1) perform patch by patch Fourier Analysis on the visual scene. It has been suggested that if V1 neurons perform patch-by-patch Fourier Analysis, then the receptive field sizes will remain constant. If this is the case, then to obtain the range of peak spatial frequencies reported for the same visual field, the neurons will have different number of sub-regions. Alternately, different peak spatial frequencies can also be obtained by keeping the number of sub-regions the same and changing the receptive field sizes. In this chapter, we will examine which of the above models best explain the receptive field properties of tree shrews. We measured the spatial frequency tuning curves of the neurons and calculated absolute and relative bandwidths. We found that the relative bandwidth was negatively correlated with the peak spatial frequency, suggesting that the shrew V1 neurons, while not ideal, are far better Fourier Analysers than the macaque V1.

7.2 Introduction

In their seminal paper, Hubel and Wiesel divided cortical neurons into simple and complex cells. While both these types of neurons were orientation selective, they were different in some key ways. Specifically, Hubel and Wiesel described simple cells as neurons that have a) spatially segregated on and off regions, b) summation within each region, c) had ON and OFF subregions that were antagonistic d) it was possible to predict the neurons response to any stimulus Complex cells were neurons that did not have the above properties. In recent years, this has been interpreted as simple cells being linear, X-like neurons while complex cells exhibit non-linear, Y-like responses. It was proposed by Robson and Campbell that neurons in the primary visual cortex function do not all function as a single detector. Rather, they suggest that there are a number of independent detector mechanism each of which is tuned to a narrow range of frequencies (Campbell and Robson, 1968). They also report that there are individual channels for most of the spatial frequencies that the neurons see. as patch by patch Fourier transformers. What this essentially meant was that neurons analysed each patch of the visual field individually and extracted the spatial frequency information and then used this information to create a composite whole. Campbell and Robson reframed this hypothesis to say that this implied that neurons that analysed the same patch of visual field had the same receptive field sizes but different peak spatial frequencies. This is supported by studies that have shown that

in the primary visual cortex, while there are orientation columns where the orientation remains constant, there are no such spatial frequency columns. Within an area of the cortex, spatial frequency can vary by a lot. For neurons to have the same receptive field size but different peak spatial frequencies, they should have different number of receptive field sub-regions. Blah blah blah showed that the size of the receptive subregions affect the peak spatial frequencies whereas the number of receptive field sub-regions affects the bandwidth of the tuning (see figure 1a an). This implies that if the receptive field size remains constant, the only way we could achieve different peak spatial frequencies will be by changing the size of the sub-regions. This would mean that as the peak spatial frequency increases, the size of subregions decrease and the number of sub-regions increase which also means that the spatial frequency tuning bandwidth gets narrower (rows 1 and 2 of figure 1). Alternately, we could achieve the same results by keeping the same number of sub-regions but by changing receptive field sizes as shown in figure 1b and c. In this case, the relative bandwidth of the spatial frequency tuning would remain constant even as the peak spatial frequency increases. In the cats and macaques, this second model of constant relative sub-regions has been shown to be true (Vidyasagar and Kulikowski, 1986; Kulikowski and Bishop, 1981). In the tree shrews, while orientation selectivity has been widely studied, very few studies have been conducted on the spatial frequency selectivity of the tree shrew V1. One study looked at the distribution of spatial frequency between layers 2/3 and layer 4 and found that most neurons in layer 2/3 showed

band-pass spatial frequency tuning with neurons predominantly showing a tuning bandwidth of 2 octaves. Apart from this one study, no other reports of spatial frequency tuning has been shown. Our own results are similar to previously reported results on the layer 2/3 neurons (see Previous chapter). We also found that compared to layer 4, more neurons were likely to be band-pass tuned for spatial frequency. Here we aimed to examine the relationship between the orientation tuning bandwidth and the peak spatial frequency.

Simple cells as patch by patch Fourier Analysers

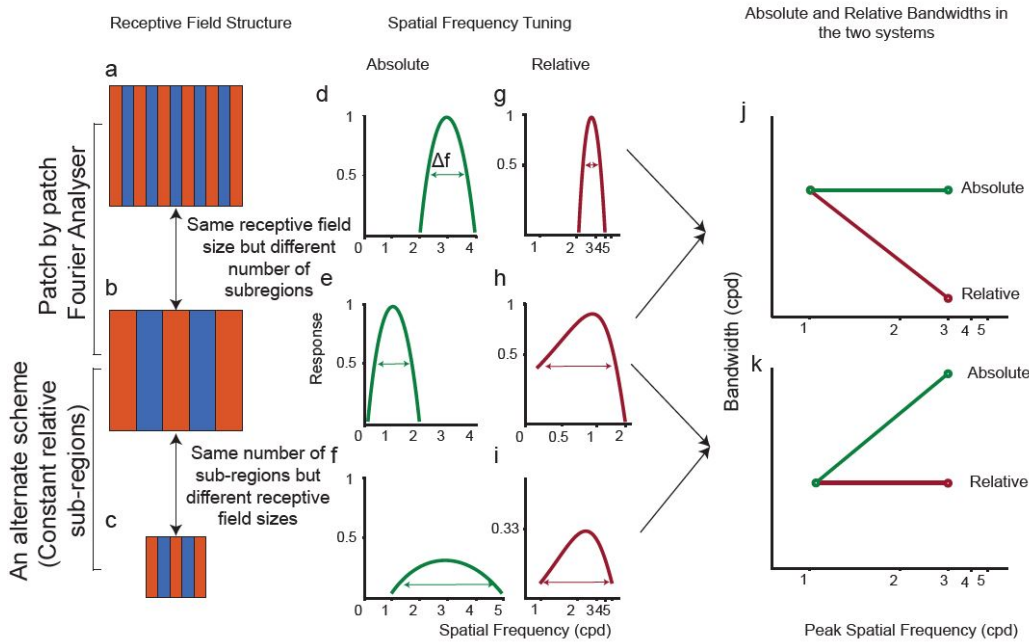


Figure 7.1: Distribution of segregation indices of neurons.

As mentioned earlier, neurons in the primary visual cortex can be classified as simple or complex cells. The criteria mentioned by Hubel and Wiesel

(1962) are all subjective methods of classifying cells into simple cells. Since then, more objective methods of classifying receptive fields into simple and complex have been established. The first method is by calculating the modulation index (MI). The MI is the ratio between the DC and first harmonic component of the temporal modulation neurons exhibit when shown drifting gratings. This method quantifies the linearity of a neurons response based on the assumption that simple cells show linear summation within their receptive field sub-regions. Skottun et al (1991) showed that this method successfully divided neurons into two groups which were roughly the same as simple and complex cells divided using the criteria specified by Hubel and Wiesel (1962). While the modulation index measured the linearity of the neurons in cats, in macaques and tree shrews, it tended to overestimate the number of simple cells found. In tree shrews, while over 40% of neurons could be classified as simple using the modulation index, these neurons did not show the segregation of receptive field sub-regions requisite of simple cells (Van Hooser et al., 2013; Veit et al., 2014). This has also been shown to be the case in macaques (References). Further, it has also been suggested that linearity is not a requisite feature of simple cells. Neurons in the LGN maybe classified as X, Y and W cells. While X cells show linear sustained responses, Y cells exhibit transient, non-linear responses. While originally thought that X and Y cells projected to simple and complex cells respectively, this connection has since been disproved. As a result, significant non-linearities may be introduced in simple cells depending on the type of input that they receive. Further, if

simple cells do function as edge detectors rather than linear filters, they are unlikely to be linear neurons (DeValois and Webster, 1978). Hence, alternate methods of classifying simple cells are also examined below. Whether there are cortical simple and complex cells have also been debated. Depending on stimulus parameters, there seems to be a continuum of neurons rather than a bimodal distribution of neurons in the primary visual cortex. So the linear component of all neurons have also been subjected to the same analysis.

7.3 Methods

7.3.1 Surgery and Anaesthesia

Surgical procedures are as outlined in the Methods chapter. Briefly, the animal was anaesthetized using a mixture of Ketamine and Xylazine, a venous catheter was inserted in to the femoral vein and a tracheostomy performed to assist in breathing during the experiment. The animal was administered muscle paralysant (Vecuronium Bromide) intravenously and was anaesthetised using Isoflurane (0.5-1%) for the duration of the experiment. Hard contact lenses were fitted to the eye to prevent corneal drying. In some tree shrews, additional lenses were used to correct for any refractive errors. A craniotomy and durotomy were performed over the location of V1 (Horsley-Clarke Coordinates A2.5 to P2.5). ECG and frontal EEG were monitored during the experiment. At the end of the experiment, the animal was euthanized using an overdose of pentobarbital sodium and perfused using 0.1M Phosphate

Buffer (PB) solution followed by 4% Paraformaldehyde in 0.1M PB. The brain was removed and stored in sucrose (20-25%) for histology.

7.3.2 Electrophysiology

High impedance, lacquer coated tungsten microelectrodes (FHC Metal Microelectrodes Inc., ME, USA; impedance= 12-18 M) were lowered into the brain at an angle perpendicular to the cortical surface. The signal was amplified and filtered (x 10,000 gain, bandpass filtered between 300-3000 Hz, A-M systems) and fed into an audio speaker as well as an analog to digital converter (Cambridge Electronic Design Limited, Cambridge, UK; digitised at 22.5 kHz). Neurons were recorded from Layers 2/3 and Layer 4. Layer 4 could be identified by a characteristic swish, first for on stimuli and then for off stimuli, in the tree shrews. Where we no longer heard the swish, we concluded that we exited layer 4 and into layer 5. Neurons in layers 5 and 6 were not recorded from. Lesions (6 A for 6s) were made at the end of each track. The electrode was withdrawn and lesions were made at regular intervals to trace the path of the electrode through the brain. The data was recorded as a spike trace using the spike 2 software (CED, Cambridge, UK). The spikes were templated and the spike timing exported as a text file. Further analysis was performed using custom MATLAB code (The Mathworks Inc, USA).

7.3.3 Stimuli

A hand-held projectoscope was used to mark the receptive field boundaries. Using this, the centre of the monitor was aligned with centre of the receptive field prior to stimulus presentation. Stimuli were presented using a BARCO monitor (Frame Refresh Rate= 80 Hz; Reference Calibrator Plus; Barco Video and Communications, Belgium) and generated using Visage (VSG, Cambridge Research Systems, Cambridge, UK) and custom Stimulus Description Language (SDL) scripts. The monitor had a mean luminance of 32.6 cdm-2. While recording, the monitor was placed at a distance of 114 cm from the eye. For each of the different stimuli described below, ten complete stimulus presentations were completed.

Bar Stimuli

For each neurons, an initial estimate of optimum orientation was obtained using bars, moving bi-directionally across the screen. The background was a uniform gray screen. Depending on the polarity of the neurons, either a bright bar or a dark bar was used (contrast= 100 %). The bar was usually 8o long (ranging between 4 and 8 degrees) and 0.5o wide (ranging between 0.1 and 1 degree). A total of 18 different orientations were tested and PSTHs (see methods) were made online using the Spike 2 software. The orientation that yielded the highest firing rate was used for further testing. After determining optimum orientation, bidirectional, dark and light (decreasing and increasing contrast) bars of the optimum orientation were used to get the response

profile of the neurons to opposite polarities (see Fig. 1).

Grating Stimuli

For all neurons, once optimum orientation was determined, spatial frequency tuning of the neurons were studied. Drifting sine-wave gratings (TF= 4Hz, Contrast=100%) of increasing spatial frequencies (between 0 and 2.2 cpd) and in the optimum orientation were presented to neurons. The responses were recorded and stored for further analysis.

7.3.4 Data Analysis

Regardless of the stimulus presented, the following analysis was performed on the extracellular trace before any specific analysis was undertaken. Spikes were templated and the spike time and stimulus markers were exported into text files. Using custom scripts in MATLAB, PSTHs (bin-width= 20ms) were constructed for each of the stimulus conditions. Spike density functions were created using a moving Gaussian envelope with of 60 ms (3 bins). This SDF was used for further analysis.

Analysis of Bar Stimuli Responses

Orientation tuning was analysed and presented in an earlier chapter. Here is the method by which the dark and light bar data was analysed.

Calculating Segregation Index (SI) For neurons where dark and light bar data was available, the segregation index (SI) was calculated using the following formula:

$$SI = \frac{\sum |R_{ton} - R_{toff}|}{\sum |R_{ton} + R_{toff}|}$$

Where, R_{ton} is the response of the neuron to a light bar and R_{toff} is the response of the neuron to a dark bar (see figure 1). The resulting value was a number between 0 and 1. Neurons with high segregation index (>0.5) were more likely to have segregated dark and light sub-regions and were hence categorised as simple cells. Likewise, neurons with low segregation indices were classified as complex cells as they were less likely to have segregated dark and light sub-regions.

Analysis if Grating Stimuli Responses

For all neurons, a discrete fourier transform was applied to the PSTH using the MATLAB fast fourier transform algorithm (FFT). The DC (F0) and the first harmonic component (F1) of the response was used for further analysis. Optimum spatial frequency for the neurons was determined as explained in Chapter 4. The modulation ratio was then calculated as follows.

$$\text{ModulationIndex}(MI) = 2 * \frac{F_1}{(F_1 + F_0)}$$

Where Rf1 and Rf0 are the responses of the F0 and F1 components at the peak spatial frequency. The modulation ratio returned a number between 0

and 2. If the neuron had a modulation index greater than 1, it was classified as simple and it was classified as complex otherwise (Van Hooser et al., 2013). Only neurons classified as simple cells were used for further analysis and only the F1 component of the responses were further analysed. For each neuron, two spatial frequency tuning bandwidths were calculated. One was the absolute bandwidth which was the difference between the upper and lower cutoff spatial frequencies. The upper cut off was calculated as the spatial frequency greater than the peak spatial frequency where the response first reaches half the maximum response. The lower cutoff was calculated similarly for spatial frequencies lower than peak spatial frequency where response first reached half the maximum response. If the response never reached half the maximum response, the neuron was classified as low pass or high pass tuned. The relative bandwidth was then calculated as the absolute bandwidth/ peak spatial frequency.

7.3.5 Histology

The brains were stained for Nissl substances using cresyl violet acetate and lesions were located. The number of neurons found in each layer have been presented in V1 chapter and are not presented here. However, for all the results presented here, layer specific results are also presented.

7.4 Results

Results from a total of 64 neurons are presented below. Where possible, the layerwise distribution is also presented.

Segregation Index In 49 of the 64 neurons, we recorded the response of the neuron to dark and light bars. Simple cells have segregated receptive fields which appear as separate peaks in the PSTHs (Fig 1a) and complex cells have overlapping subregions which appear as overlapping peaks in the PSTH (Fig 1b). Accordingly, the segregation index is higher for simple cells compared to complex cells.

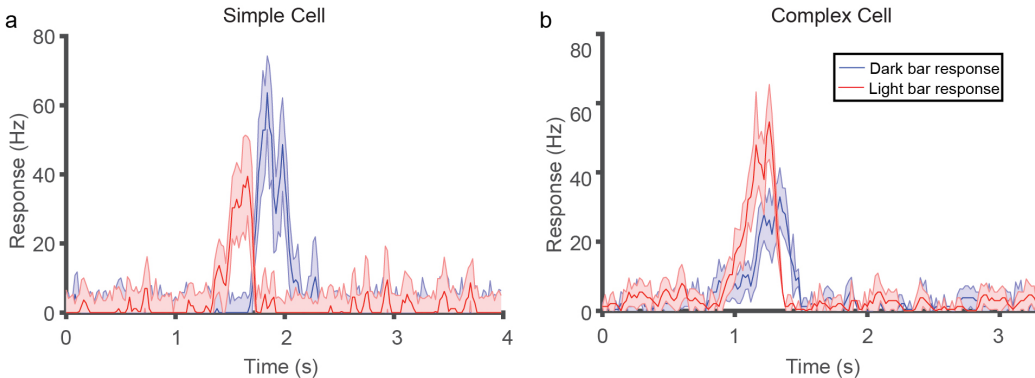


Figure 7.2: Response of a simple (a) and complex cell (b) to the dark and light bar stimuli. The spatially segregated RF of the simple cells is translated into the temporally segregated response of the neuron. Whereas, in the complex cell, the overlapping sub-regions are reflected in the temporally overlapping response of the neuron. Accordingly, the simple cell has a high SI (0.92) and the complex cell has a lower SI (0.39).

The distribution of segregation index for 47 neurons is presented below. Of the 49 neurons, 19 were from layer 2/3, 12 were from layer 3c and 18 were from layer 4. There was no significant difference in SI between the layers (Kruskal-Wallis test, $p=0.34$).

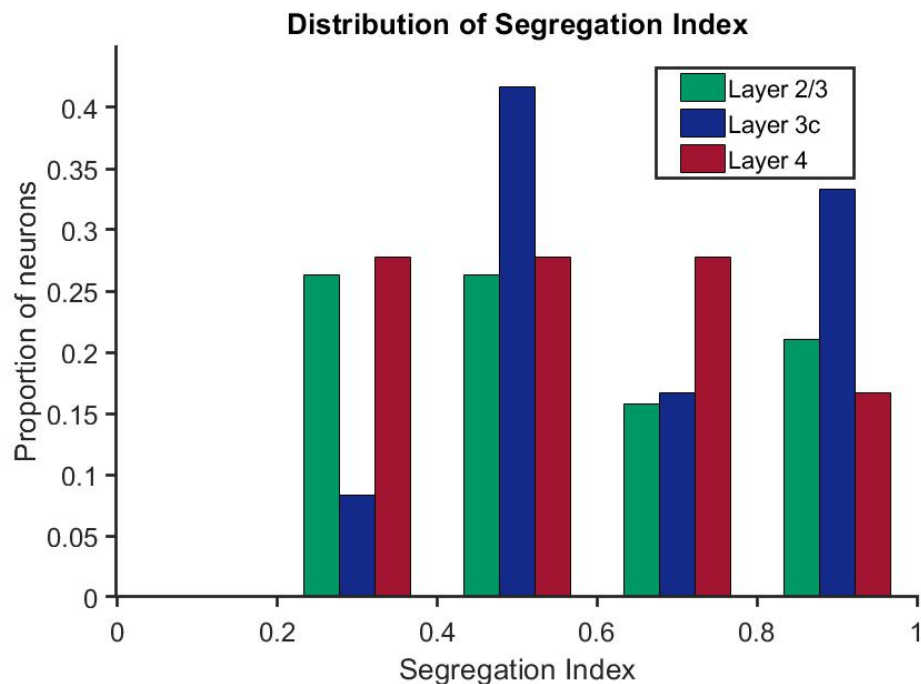


Figure 7.3: Distribution of segregation indices of neurons.

Modulation Index The modulation indices of all the 69 neurons [Layer 2/3= 27; Layer 4= 27; Layer 3c= 15] are shown in figure 3. There was no significant difference in the modulation index between the layers (Kruskal-Wallis test, $p= 0.74$).

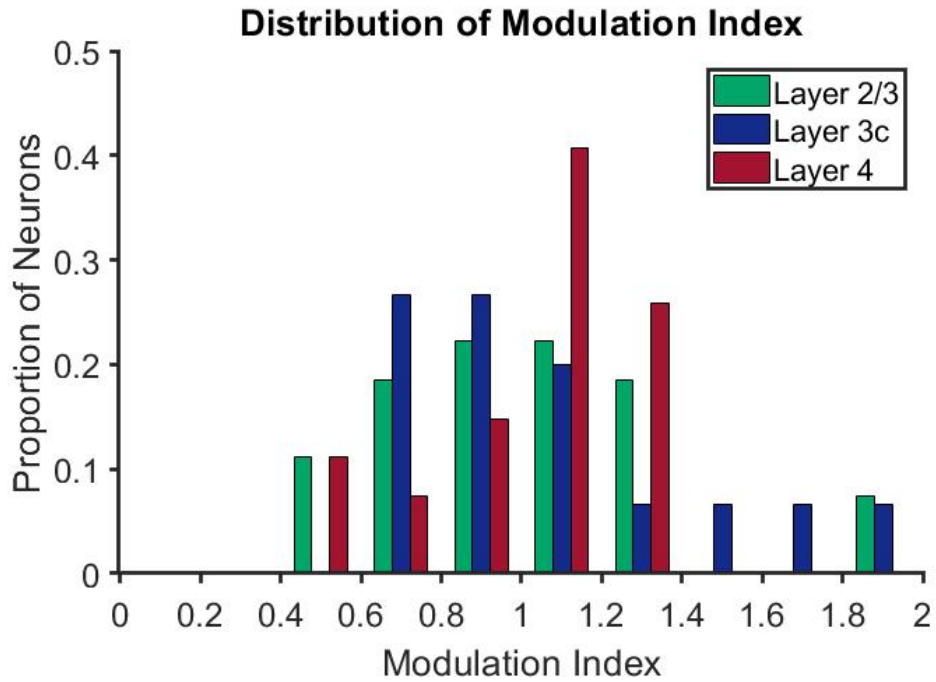


Figure 7.4: Distribution of modulation indices of neurons.

In neurons where both the segregation index and modulation index were recorded, they were plotted against each other. There was no significant correlation between the two indices ($\rho=0.02$, $p=0.89$).

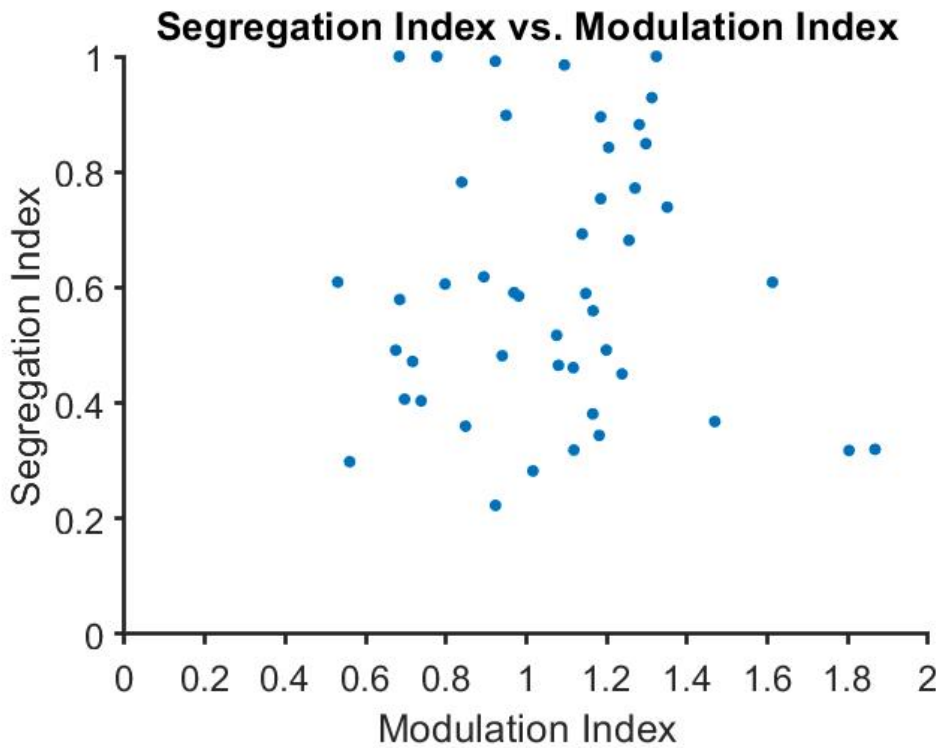


Figure 7.5: Relationship between the modulation and segregation indices.

Relationship between bandwidth and spatial frequency Neurons were classified as simple cells using the modulation index ($MI \geq 1$), the segregation index ($SI \geq 0.5$), both the modulation and segregation index together ($MI \geq 1$ and $SI \geq 0.5$). The relationship between the absolute bandwidth and the peak spatial frequency for simple cells classifies as described as above as well as for all the neurons in the sample are shown in figure 5(a,c,,e & g). Statistically significant relationships are indicated using *. For the other two measures used for classification, the correlation was not significant. There

was a significant correlation between the when all neurons were used for the analysis. The relationship between relative bandwidth and the peak spatial frequency are shown in the right hand panel. In all cases except for the one in (f) the results were statistically significant.

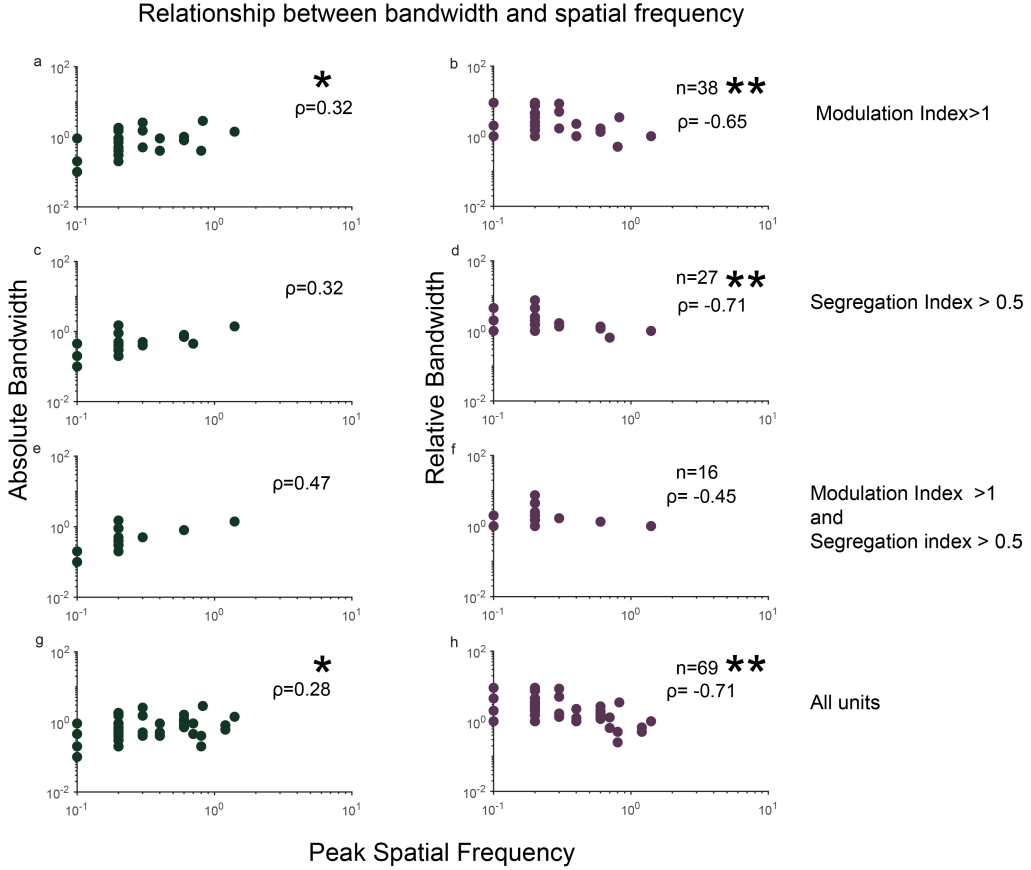


Figure 7.6: This figure shows the relationship between bandwidth and spatial frequency in simple cells when using the modulation index to classify units (a,b), when using the segregation index (c,d); using both the modulation and segregation index (e,f) and for all neurons in the sample (g,h). The plots on the left hand side show the relationship between absolute bandwidth and the peak spatial frequency while the plots on the right hand side show the relationship between the relative bandwidth and peak spatial frequency. Number of units used for generating each plot is specified in the right hand corner and statistically significant results are shown by *. * $= p<0.05$. ** $= p<0.0001$.

7.5 Discussion

In this chapter, we investigated whether neurons in the tree shrew V1 behaved like patch by patch Fourier analysers. Our results show while most simple cells do not behave like ideal Fourier analysers, they are still far better Fourier analysers than the neurons in cat and macaque striate cortex.

In order to classify the neurons into simple and complex cells, we used two objective measures that are regularly used in the literature: a) The Segregation Index and b) The Modulation Index. The SI measures the degree of separateness of the receptive field sub-regions i.e., if there are separate on and off sub-regions. Using this measure, we found that about half the neurons for which this data was available were simple. The MI on the other hand measures the degree of linear summation over the receptive fields. Using this measure too, a similar proportion of neurons were classified as simple cells. However, there was no significant correlation between the two measures (See fig.7.5). This indicates that different neurons are classified as simple based on the two different measures. Only half the neurons that were classified as simple using the SI were also classified as simple using the modulation index, indicating that atleast half the neurons that show linear summation over their receptive field also had overlapping sub-regions.

Of the neurons that were classified as simple using both MI and SI, there was no statistically significant correlation between the peak spatial frequency and the absolute bandwidth. However, this doesn't necessarily mean that

these neurons do not function as Fourier analysers. A power analysis showed that for an expected correlation of -0.45, the sample size had to be atleast 36 for a statistically significant result. It could simply mean that there was not enough neurons in our sample.

The distribution of SI and MI in our results show that neither of these values differ significantly across layers. The SI seems to be distributed almost uniformly across the whole range of possible values (between 0 and 1). However, it is interesting to note that no neurons showed complete and equally overlapping subregions ($SI < 0.2$; see fig.7.3). These results are also consistent with those published by Van Hooser et al., 2013 (see fig 3c). This could mean that most neurons in the shrew V1 receive unbalanced on and off inputs. (Check Bimodality Index). Previous studies have suggested that the tree shrew V1 has a preponderance of off dominated neurons. It has also been suggested that this off dominance could be the origin of orientation selectivity in the V1 of tree shrews. Another reason for the difference could also be the way SI is calculated. The SI is calculated from the temporal profile of the neuronal response to light and dark bars. While this gives an accurate enough measure, it may not be sensitive enough to detect small differences in sensitivities between the off and on regions.

While the distribution of MI was not significantly different between the layers, there are a few important trends that may be of note. First, while the layer 2/3 and layer 3/c distribution look identical, a majority of Layer 4 neurons seem to have a modulation index greater than 1 (see fig.7.4). This

is consistent with reports in literature where the simple cells are present predominantly layer 4 with some complex cells also found in this layer. However, a significant proportion of layer 2/3 and layer 3c neurons are also highly modulated, simple like neurons, which are reported only rarely in the literature (References).

Here we used a modified version of the modulation ratio (F_1/F_0) to quantify the degree of linear summation within the receptive field. In the original modulation ratio, neurons were only classified as simple if their F_1/F_0 ratio was greater than 1.57 (Skottun et al., 1991; Movshon et al., 1978). This number roughly translates to an MI of 1.2. Therefore, while neurons whose MI are between 1 and 1.2 have a greater modulated component of the response compared to the unmodulated component, they still show significant non-linearities. These neurons have been classified previously as 'b' cells. In our sample, we also found that these neurons were dominated by one polarity (either on or off), which also makes sense as on and off neurons are segregated into layers in the shrew V1.

Finally, the distribution of SI and MI observed in our data also calls into question the age old question of whether simple and complex cells are two separate categories of neurons or if they lie on a continuum. Our data shows that both these measures are unimodally distributed and not bimodally distributed in line with previous studies which have suggested a similar pattern. Further, it has also been suggested that under certain circumstances, simple could behave like complex cells and complex cells could behave like simple

cells. This property of neurons has been implicated in their ability to transmit signals; i.e., simple cells will behave like simple cells when their output is relevant for perception but not otherwise.

Plan: 1) Summary of results Differences in modulation index and segregation index. What this means? Linearity of neurons? Segregation index: no neurons that had completely overlapped sub-regions i.e. $si \geq 0.2$. with the rest of the SI, evenly distributed across the layers. There was no significant differences between layers.

Modulation index: Although not statistically significant, modulation index ≤ 1 for most layer 2/3 and layer 3c. modulation index ≥ 1 . Most layer 4 neurons, have a modulation index between 1 and 1.2. This is the equivalent of between 1 and 1.57 using the standard modulation ratio calculated ($F1/F0$). These neurons still have a higher modulation index but not high enough. Could be potential B cells described by Henry et al or the non-linear simple cells described by other people.

Simple cells are found in input layers while complex cells are found in supragranular layers. True if we look at the modulation index but not when looking at the segregation index. Provides support against the hierarchical model of visual processing where simple cells project to complex cells. Also has been shown in other species- complex cells are found in layer 4 and simple cells in supragranular layers. We see the same trend here.

How do our results of segregation index and modulation index compare with the previously published results for segregation and modulation ratios?

Our results are similar to previously published results by Van Hooser et al., 2013. Both results seem to show a unimodal distribution with a range of linearities in the receptive fields when compared to a simple/complex bimodal distribution. Is this because of the measure used for modulation index? Checked with regular modulation index (F_1/F_0) This measure also did not yield a bimodal distributions.

What does the relative bandwidth and spatial frequency relationship mean?

We found that in most cases, there was a negative relationship between the pk spatial frequency and the relative bandwidth of the neurons, especially when the linear component of all the neurons were used to run the analysis. This means that most neurons in the shrew V1 actually do act as linear filters in optimum range of the neurons (See Fig.7.1). What exactly does this mean? The cortex could be completely throwing out this information when non-linear?

What is linearity even useful for? Are there simple and complex cells in the shrew cortex? Does this mean anything?

References

Swisher, J. D., Gatenby, J. C., Gore, J. C., Wolfe, B. a., Moon, C.-H., Kim, S.-G., & Tong, F. (2010, jan). Multiscale pattern analysis of orientation-selective activity in the primary visual cortex. *The Journal of neuroscience : the official journal of the Society for Neuroscience*, 30(1), 325–30. Retrieved from <http://www.ncbi.nlm.nih.gov/pmc/articles/PMC2823298/> doi: 10.1523/JNEUROSCI.4811-09.2010